

# Extragalactic Point Source Search in Five-year WMAP 41, 61 and 94 GHz Maps

X. Chen & E. L. Wright

*Physics and Astronomy Department, University of California, Los Angeles, CA 90095-1547*

## ABSTRACT

We present the results of an extragalactic point source search using the five-year WMAP 41, 61 and 94 GHz (Q-, V- and W-band) temperature maps. This work is an extension of our designing and applying a CMB-free technique to extract point sources in the WMAP maps. Specifically, we have formed an internal linear combination (ILC) map of the three-band maps, with the weights chosen to remove the CMB anisotropy signal as well as to favor the selection of flat-spectrum sources. We have also constructed a filter to recover the true point source flux distribution on the sky. A total of 381 sources are found in our study at the  $> 5\sigma$  level outside the WMAP point source detection mask, among which 89 are “new” (i.e., not present in the WMAP catalogs). Source fluxes have been calculated and corrected for the Eddington bias. We have solidly identified 367 (96.3%) of our sources, the  $1\sigma$  positional uncertainty of which is  $2'$ . The 14 unidentified sources could be either extended radio structure or obscured by Galactic emission. We have also applied the same detection approach to simulated maps, which yielded  $364 \pm 21$  detections on average. The recovered source distribution  $N(> S)$  agrees well with the simulation input, which proves the reliability of this method.

*Subject headings:* catalogs — cosmic microwave background — cosmology: observations — methods: data analysis

## 1. Introduction

The Wilkinson Microwave Anisotropy Probe (WMAP) is designed to advance observational cosmology by making precise measurements of the cosmic microwave background (CMB) anisotropy (Bennett et al. 2003a). The characterizing and removing of foreground emission play a vital role in the interpretation of CMB temperature maps. At small angular scales, extragalactic radio sources, especially those with flat spectra, constitute the

most important foreground. Therefore, it is essential to have efficient source detection techniques developed and applied to the WMAP maps. Meanwhile, since WMAP provides the only all-sky millimeter survey, source extraction in its maps also opens a window to study extragalactic radio sources in the millimeter wavelength region.

With every WMAP data release, a catalog is provided of the brightest point sources in the WMAP maps. The detection procedure used by the WMAP science team features a filtering of the integration-time-weighted maps with  $b_\ell / (b_\ell^2 C_\ell^{CMB} + C_\ell^{noise})$  in harmonic space and a search for  $> 5\sigma$  peaks, where  $b_\ell$  is the transfer function of the WMAP beam response (Page et al. 2003, Jarosik et al. 2007, Hill et al. 2009),  $C_\ell^{CMB}$  is the CMB angular power spectrum and  $C_\ell^{noise}$  is the noise power. This procedure successfully generated 208, 323 and 390 point sources in the WMAP first year, three-year and five-year maps, respectively (Bennett et al. 2003b, Hinshaw et al. 2007, ?; hereafter, WMAP1, WMAP3 and WMAP5 catalogs). However, because of the limited angular resolution of WMAP, positive CMB excursions can be confused with point sources. In addition, the  $C_\ell^{CMB}$  term in the filter counts as a systematic noise that does not integrate down with observing time. This largely limits the increasing of the number of detections with increased sensitivity of the maps. To circumvent the CMB “noise”, Chen & Wright (2008) introduced a CMB-free technique, which involves forming internal linear combination (ILC) of multi-frequency maps to suppress the CMB signal. The number of sources  $N$  found by applying this technique to the WMAP V- and W-band maps alone varied as  $t^{0.72}$  from one year to five years, in comparison to  $N \sim t^{0.39}$  between the WMAP1 and WMAP5 catalogs (Wright et al. 2009).

In this paper, we extend this CMB-free technique and employ it to the WMAP five-year Q-, V- and W-band temperature maps. The main goal is to utilize the high signal-to-noise ratio Q-band data to find more flat-spectrum sources, which are known to dominate the 30 - 100 GHz frequency regime.

## 2. Methodology

### 2.1. Point Source Detection

The WMAP temperature maps at HEALPix<sup>1</sup> Res 9 are used in this study. To minimize the noise difference between maps, we first smooth the high resolution V- and W-band maps

---

<sup>1</sup>The Hierarchical Equal Area isoLatitude Pixelization (HEALPix) of the sphere is used to define WMAP map pixels on the sky in Galactic coordinates. Res 9 corresponds to 3,145,728 pixels over the full sky with a pixel resolution of 0.115°. See more of HEALPix at <http://healpix.jpl.nasa.gov/>.

to match the Q-band resolution. We construct the smoothing functions using a polynomial of an infinitely smooth function with compact support, i.e.,

$$S(\theta) = \sum_n a_n S_n(\theta), \quad (1)$$

where

$$S_n(\theta) = \begin{cases} \exp(-\frac{n\theta^2}{\theta_{Rc}^2 - \theta^2}) & \theta < \theta_{Rc} \\ 0 & \theta > \theta_{Rc}. \end{cases} \quad (2)$$

The coefficients  $a_n$ 's are fitted by requiring the Legendre transform of the smoothing functions to match the ratios of Q-band beam transfer function to V-band and W-band beam transfer functions separately. And a cutoff radius  $\theta_{Rc}$  of  $1.25^\circ$  is chosen for the solid angle integrations.

We then form the ILC map out of the Q-band map, V-band smoothed map and W-band smoothed map,

$$T^{ILC} = \omega_Q T_Q + \omega_V T_V^{SM} + \omega_W T_W^{SM}. \quad (3)$$

The weights are determined by canceling out the CMB anisotropy signal

$$\omega_Q + \omega_V + \omega_W = 0, \quad (4)$$

normalizing the flat-spectrum source flux to the Q-band

$$\omega_Q + \omega_V \left( \frac{\partial B_Q}{\partial T} / \frac{\partial B_V}{\partial T} \right) |_{T_0} + \omega_W \left( \frac{\partial B_Q}{\partial T} / \frac{\partial B_W}{\partial T} \right) |_{T_0} = 1, \quad (5)$$

and minimizing the variance of the combination map, which can be approached by minimizing  $(\omega_Q^2 + \omega_V^2 + \omega_W^2)$  since the variance at each pixel is approximately the same for Q, V and W bands. Here  $B_\nu$  is the Planck function and  $T_0 = 2.725 \pm 0.002$  K is the CMB temperature (Mather et al. 1999). The three-band ILC map is shown in Figure 1a.

For any pixel  $i$  within the Q-band beam to a point source, assuming negligible contribution from the overlap of point sources, its temperature  $T_i^{ILC}$  in the ILC map can be fitted into the point source intensity  $f$ , multiplied by the beam response at that pixel location  $b_i^Q$ , plus a local baseline  $c$ , i.e.,

$$T_i^{ILC} = f b_i^Q + c. \quad (6)$$

Deviation from the fit is evaluated using the  $\chi^2$ ,

$$\chi^2 = \sum_{ij} \epsilon_i (N_{ij}^{-1}) \epsilon_j, \quad (7)$$

where

$$\epsilon_i = T_i^{ILC} - (f b_i^Q + c) \quad (8)$$

and

$$N_{ij} = \delta_{ij}\sigma_Q^2\omega_Q^2 + \sum_k S_{ik}^{V2Q} S_{jk}^{V2Q} \sigma_V^2 \omega_V^2 + \sum_k S_{ik}^{W2Q} S_{jk}^{W2Q} \sigma_W^2 \omega_W^2. \quad (9)$$

Here  $S^{V2Q}$  and  $S^{W2Q}$  are the smoothing functions used to smooth the V-band and W-band maps previously; the summation over  $k$  is a sum over all the pixels within  $\theta_{R_c}$  of pixel  $i$  and  $j$ ;  $\sigma_Q$ ,  $\sigma_V$  and  $\sigma_W$  are the noise at pixel  $k$  in the Q-, V- and W-band maps, respectively. The best fit is defined when the  $\chi^2$  reaches a minimum, which gives

$$\sum_{ij} N_{ij}^{-1} \begin{pmatrix} b_i^Q \\ 1 \end{pmatrix} \begin{pmatrix} b_j^Q & 1 \end{pmatrix} \begin{pmatrix} f \\ c \end{pmatrix} = \sum_{ij} N_{ij}^{-1} T_j^{ILC} \begin{pmatrix} b_i^Q \\ 1 \end{pmatrix}. \quad (10)$$

Solving the above equation, we find that the intensity of the point source can be written as a weighted sum of the intensities of its surrounding pixels, i.e.,

$$f = \sum_j \left[ \sum_i (M^{-1})_{00} b_i^Q N_{ij}^{-1} + \sum_i (M^{-1})_{01} N_{ij}^{-1} \right] T_j^{ILC}, \quad (11)$$

where

$$M = \sum_{ij} N_{ij}^{-1} \begin{pmatrix} b_i^Q \\ 1 \end{pmatrix} \begin{pmatrix} b_j^Q & 1 \end{pmatrix}. \quad (12)$$

Since the weights inside the square brackets of Equation (11) are essentially a function of the angular distance to the considered source, this suggests that we can probe the point source flux in the ILC map by fitting the function and filter the map locally. As a first attempt, we generate 32 random source positions in the sky and for each position calculate the weights to a distance of  $1.25^\circ$ . We plot the weights against the angular distances at each selected random spot, and note that they all share the same profile. This leads us to fit a single function using the collective weights from the 32 random positions. Convolution of the all-sky ILC map with this global filter, we are able to recover the point source flux distribution on the entire sky, shown in Figure 1b. The extreme negative regions in the map are regions surrounding the brightest sources, where fluxes in the pixels are depleted and restored into their central point sources by filtering.

We adopt the same Kp0+LMC+SMC detection mask used by the WMAP team (Wright et al. 2009, shown as contours in Figure 1b) to exclude extended foreground emission. Following the WMAP scan pattern that gives non-uniform observation numbers among pixels: greatest at the ecliptic poles, high at latitude  $\pm 45^\circ$ , and least in the ecliptic plane, we divide the masked sky into rings that cover 1 degree in ecliptic latitude. We then compute  $\sigma$  individually within each ring and look for peaks greater than  $5\sigma$ . When more than one  $> 5\sigma$  pixel lay within a  $3 \times 3$  pixels area, the brightest one is chosen as a source detection. The accurate

source position is approached by fitting a point source profile to the 9-pixel grid centered on the brightest pixel and defined at where the peak is. We find 381 sources in our study. The distribution of these sources on the sky is given in Figure 2; Blue, green and red dots indicate, respectively, sources in the WMAP catalogs, newly detected and identified, and newly detected but unidentified (See §2.3 for a detailed discussion of source identification).

## 2.2. Flux Estimation

We estimate the Q-, V- and W-band flux densities of our sources by calculating

$$F_\nu = \int I_\nu \psi(\theta) \cos \theta d\Omega = \frac{\partial B_\nu}{\partial T}|_{T_0} \int T \psi(\theta) \cos \theta d\Omega, \quad (13)$$

where  $B_\nu$  is again the Planck function and  $T_0$  is the CMB temperature of  $2.725 \pm 0.002$  K.  $T$  is the temperature measurement in each band; the solid angle is integrated to a radius of 1.25 degree. We have introduced a weighting function  $\psi(\theta)$  in our flux estimator to help enhance the contrast of the point source flux to the background. This function is constructed individually in each band with the corresponding beam profile in the center and a negative Gaussian ring in the outer field. We require

$$\int \psi(\theta) d\Omega = 0, \quad (14)$$

in order to ignore any flux that spreads uniformly across the whole integration field. The mean and variance of the Gaussian functions are optimized to preserve the source flux while minimizing the fluctuation in the integration field:

$$\sigma^2 = \sum_i \sum_j \psi_i \psi_j (C(\theta_{ij}) + \delta_{ij} N_i), \quad (15)$$

where

$$C(\theta) = \sum_\ell \frac{2\ell + 1}{4\pi} C_\ell \omega_\ell P_\ell(\cos\theta). \quad (16)$$

Here  $i$  and  $j$  denote pixels within the integration field;  $N$  is the radiometer noise in the five-year maps;  $C_\ell$  is the best fit power spectrum of WMAP5 data assuming a  $\Lambda$ CDM model;  $\omega_\ell$  is the window function which encodes the beam smoothing (Page et al. 2003);  $P_\ell$  is the Legendre function. We see negative fluxes for some sources, which is likely caused by our source sitting on the top of a negative CMB fluctuation. The error on the flux density is calculated as the flux rms value of the background pixels that are close to the target source but are not “contaminated” by it. Specifically, we select a ring of pixels around the source

with an inner radius equal to  $1^\circ$  to exclude pixels affected by the source fluxes, and an outer radius of  $2^\circ$  to include sufficient number of pixels to estimate the background fluctuation level.

Since flux estimates of sources in noisy fields are on average overestimated (Eddington Bias, Eddington 1940), we have applied the Bayesian approach described in the Appendix B of López-Caniego et al. (2007) to correct for the bias. The estimated slopes of the differential number counts are 2.67, 2.68 and 2.30 for the Q, V, and W bands separately. We compare the uncorrected fluxes of each band with the corrected ones in Figure 3. The agreement is generally good, and the correction makes almost no difference for fluxes  $\gtrsim 1.5$  Jy in Q and V bands.

### 2.3. Identification

We search in the NASA/IPAC Extragalactic Database (NED<sup>2</sup>) and the source catalogs from two recent all/large sky radio surveys: CRATES (8.4 GHz, Healey et al. 2007) and the Australia Telescope 20 GHz Survey (AT20G, Massardi et al. 2008), for radio sources within  $15'$  ( $\theta_{FWHM}^Q \sim 30.6'$ ) to our sources. We retrieve the available photometric data and make the spectral energy distribution (SED) plots for these radio sources. If the flux densities of our source can be reasonably fitted into the SED of a known radio source, we associate them. This SED approach identifies 367 (i.e. 96.3%) sources on our list, the majority of which are found to have a flat spectrum, i.e.,  $\alpha \sim 0$  in  $F_\nu \sim \nu^\alpha$ . This is consistent with our knowledge of the dominance of flat-spectrum sources in this wavelength regime, and with the weights we chosen for the ILC map that favors flat-spectrum sources. Nevertheless, we do detect some steep-spectrum sources as well as sources with spectra peaked at  $\sim 10$  GHz (see Figure 4 for some SED examples). We have also searched NED for the optical identifications of our sources and found 269 QSOs, 61 galaxies, 1 galaxy pair, 1 galaxy triple, 1 planetary nebula and 34 unclassified radio sources among the identified ones. Additionally, NED provides redshifts for 306 identified sources. A plot of the redshift distribution of these sources is given in Figure 5, the median of  $z$  is 0.85.

We then cross-correlate our list of identified sources with the WMAP catalogs. If a source is within  $15'$  of a WMAP cataloged source, we tag it. We find 287 of our sources present in the WMAP5 catalog, and five more sources (J0734+5026, J1513-1013, J1553-7914, J1644-7713, J1648+4109) are in the WMAP3 catalog but missing from the WMAP5 catalog. The high associate rate clearly demonstrates that our method can generate results

---

<sup>2</sup>See <http://nedwww.ipac.caltech.edu/>.

consistent with the method adopted by the WMAP team. In Figure 6, we compare our flux estimates with the ones given in the WMAP catalogs. These two sets of fluxes agree very well with each other at  $F_\nu \gtrsim 1$  Jy. Our estimates are in general lower than the WMAP ones for faint sources, which is partially due to the flux correction we made. The most deviated point in both Q and V bands is Fornax A, known as an extended source with a relatively weak core and two large extended lobes. A complete list of all the identified sources is given in Table 1, sorted in ascending order of right ascension. For each source, we give its WMAP5 ID (if available), optical identification, flux densities along with  $1\sigma$  errors at the WMAP Q-, V- and W-band, its 5 GHz ID as given in GB6 (Gregory et al. 1996), PMN (Griffith et al. 1994, 1995, Wright et al. 1994, 1996), S5 (Kuehr et al. 1981a) or Kuehr et al. (1981b) catalogs, and the angular distance to its 5 GHz counterpart. For four of our sources (J0422+0212, J0721+0403, J0805+6143, J1015+2258), we have assigned different 5GHz IDs than given in the WMAP5 catalog based on the SEDs of the 5 GHz sources. The position errors of our detections are evaluated with respect to the positions of their 5 GHz counterparts since the 5 GHz surveys have in general higher angular resolutions. Assuming the source deviations from their 5 GHz counterparts in both the galactic longitude and latitude axes are normally distributed, the angular distance  $r$  to the 5 GHz IDs should satisfy a Rayleigh distribution and the radial positional uncertainty of our sources can then be estimated as  $\sigma_r = \text{median}(r)/\sqrt{\ln 4} = 2'$ . We conclude that our 5 GHz IDs are more reliable since we obtain a better positional accuracy than the WMAP5 survey (4' in both longitudes and latitudes).

There are 14 sources left without any solid identification, as listed in Table 2 and noted in red in Figure 2. Looking back into the filtered ILC map (Figure 1b), we do see bright emission features at the corresponding locations. We suggest that these sources could be either extended radio structure or obscured by Galactic emission. Considering the low or negative flux densities obtained for some of these sources, it is likely that some of them are located on the top of negative CMB fluctuations so that they do not show as strong sources in each band but show up in the CMB-free ILC map. We cross-correlate this list with the GB6, PMN, S5 and Kuehr et al. (1981b) catalogs. If a 5 GHz source is within 15', we suggest it as the possible counterpart of our source. In cases when no 5 GHz source is found nearby, we use the closest 1.4 GHz NVSS (Condon et al. 1998) source or 843 MHz SUMSS (Bock et al. 1999, Mauch et al. 2003) source instead.

### 3. Discussion

#### 3.1. Source Number Counts

We have calculated the source number counts in bins of  $\Delta \log S = 0.2$  at Q-, V- and W-band<sup>3</sup> and compared them with the predictions of the cosmological evolution model by de Zotti et al. (2005). As illustrated in Figure 7, the agreement is generally good above  $\sim 2$  Jy (i.e.,  $\log S = 0.3$ ) in the Q and V bands. The low data points at lower fluxes are due to the incompleteness of our sources at these flux ranges. In the W-band, our data points agree more with a model rescaled by 0.86. The source counts derived from WMAP5 catalog in the corresponding bands are also plotted for comparison. They are mostly consistent with the source counts in this work.

#### 3.2. Chance-Coincidence Rate

To estimate the influence of false identifications from random coincidences, we have generated an equal number (i.e., 381) of random positions outside the WMAP source detection mask. We repeat the same near-position search in NED. If a 5 GHz source is found to have  $F_\nu \gtrsim 100$  mJy within  $15'$  of a fake source position, we calculate the spectral index  $\alpha$  using the 5 GHz flux estimate along with the 1.4 GHz flux estimate from the NVSS catalog or 843 MHz flux estimate from the SUMSS catalog (all such 5 GHz sources have a NVSS or SUMSS counterpart). We then use the spectral index to extrapolate this source's 5 GHz flux to the WMAP 41 GHz channel (Q-band). We consider a source as identified when its Q-band flux is above 100 mJy. Following this approach, we associate 14 random sources with known radio sources, corresponding to a chance-coincidence rate of 3.7%. In Figure 8, we plot the distribution of position offsets of real detections to their 5 GHz counterparts, in comparison with the distribution of the identified random sources. It is evident that the false identifications with random sources generally have a larger position error than the real peak positions. Based on this plot, we suggest that our source identifications within  $5'$  are probably real.

---

<sup>3</sup>By convention,  $S$  is often used to represent the flux density in the discussion of number counts distribution; it is equivalent to  $F_\nu$  that is used throughout this paper.



### 3.3. Analysis of Simulated Maps

We repeat the same point source analysis on simulated maps constructed with point sources, CMB fluctuations, and radiometer noise.  $10^6$  sources are sampled from a power law distribution  $N(> S)$  at the WMAP Q-band (centered at 40.7 GHz), derived from WMAP5 sources with  $F_Q > 1$  Jy as they appear to be complete to  $\sim 1$  Jy (Figure 9). Spectral indices are chosen from a Gaussian with mean -0.09 and standard deviation 0.176 (Wright et al. 2009), and the fluxes are scaled to the V- and W-band centers (60.8 GHz and 93.5 GHz). In each band, we calculate the appropriate temperature of every source and assign it to a random HEALPix pixel at Res 11 (a total of  $12 \times 4^{11}$  pixels). These point source maps are then smoothed with the beam window function at each band and converted to Res 9 maps. Finally, we add in the Res 9 maps of CMB fluctuations produced using the best fit  $C_\ell$ 's from WMAP5 data assuming a  $\Lambda$ CDM model, and of radiometer noise generated from the WMAP5 noise variance in each pixel. The point source detection process is then applied to these simulated maps, yielding on average  $364 \pm 21$  point sources for the 10 simulations we completed. When compared with the input point source maps, we find only 2 spurious sources out of the total detections from our simulations. The recovered  $N(> S)$  agree remarkably well with the simulation input for fluxes  $> 1$  Jy, which infers that our method is robust and the source counts we get from the WMAP5 ILC map are reliable for fluxes  $> 1$  Jy.

## 4. Conclusions

We present catalogs of point sources found in an ILC map constructed from the WMAP five-year Q-, V- and W-band maps. We have recovered 287 WMAP5 sources and five WMAP3 sources in our survey. Bypassing of CMB “noise” in the detection process brings us 89 new sources (23.4% of the total). We have obtained flux density estimates for our sources in each of the three bands. Most of the new sources are found to have low or even negative flux estimates in at least one band, which is probably due to the coincidence of their locations with negative CMB fluctuations. This will generally lead to missing of these sources in single frequency band searches. We identify our sources by searching in NED for nearby low frequency radio sources and fitting the fluxes of our sources to their SEDs. Of all the sources we detected, we lack of solid identifications for 14. The flux estimates and number count distribution of our identified sources are comparable with those from the WMAP5 catalog, which proves our method to be complimentary to as well as consistent with the WMAP approach. Since this CMB-free technique responds rapidly as observing time increases (Wright et al. 2009), we expect a fast increase of new detections in more years

of WMAP maps.

We acknowledge the use of the Legacy Archive for Microwave Background Data Analysis (LAMBDA) to retrieve the WMAP data set. Support for LAMBDA is provided by the NASA Office of Space Science. This research has also made use of the VizieR catalog service and the HEALPix (Górski et al. 2005) package.

## REFERENCES

- Bennett, C. L., et al. 2003a, *ApJ*, 583, 1
- Bennett, C. L., et al. 2003c, *ApJS*, 148, 97
- Bock, D. C.-J., Large, M. I., & Sadler, E. M. 1999, *AJ*, 117, 1578
- Chen, X., & Wright, E. L. 2008, *ApJ*, 681, 747
- Condon, J. J., Cotton, W. D., Greisen, E. W., Yin, Q. F., Perley, R. A., Taylor, G. B., & Broderick, J. J. 1998, *AJ*, 115, 1693
- de Zotti, G., Ricci, R., Mesa, D., Silva, L., Mazzotta, P., Toffolatti, L., & González-Nuevo, J. 2005, *A&A*, 431, 893
- Eddington, A. S., Sir 1940, *MNRAS*, 100, 354
- Górski, K. M., Hivon, E., Banday, A. J., Wandelt, B. D., Hansen, F. K., Reinecke, M., & Bartelmann, M. 2005, *ApJ*, 622, 759
- Gregory, P. C., Scott, W. K., Douglas, K., & Condon, J. J. 1996, *ApJS*, 103, 427
- Griffith, M. R., Wright, A. E., Burke, B. F., & Ekers, R. D. 1994, *ApJS*, 90, 179
- Griffith, M. R., Wright, A. E., Burke, B. F., & Ekers, R. D. 1995, *ApJS*, 97, 347
- Healey, S. E., Romani, R. W., Taylor, G. B., Sadler, E. M., Ricci, R., Murphy, T., Ulvestad, J. S., & Winn, J. N. 2007, *ApJS*, 171, 61
- Hill, R. S., et al. 2009, *ApJS*, 180, 246
- Hinshaw, G., et al. 2007, *ApJS*, 170, 288
- Jarosik, N., et al. 2007, *ApJS*, 170, 263
- Kuehr, H., Pauliny-Toth, I. I. K., Witzel, A., & Schmidt, J. 1981a, *AJ*, 86, 854
- Kuehr, H., Witzel, A., Pauliny-Toth, I. I. K., & Nauber, U. 1981b, *A&AS*, 45, 367
- López-Caniego, M., González-Nuevo, J., Herranz, D., Massardi, M., Sanz, J. L., de Zotti, G., Toffolatti, L., & Argüeso, F. 2007, *ApJS*, 170, 108
- Massardi, M., et al. 2008, *MNRAS*, 384, 775

Mather, J. C., Fixsen, D. J., Shafer, R. A., Mosier, C., & Wilkinson, D. T. 1999, *ApJ*, 512, 511

Mauch, T., Murphy, T., Buttery, H. J., Curran, J., Hunstead, R. W., Piestrzynski, B., Robertson, J. G., & Sadler, E. M. 2003, *MNRAS*, 342, 1117

Page, L., et al. 2003, *ApJS*, 148, 39

Wright, A. E., Griffith, M. R., Burke, B. F., & Ekers, R. D. 1994, *ApJS*, 91, 111

Wright, A. E., Griffith, M. R., Hunt, A. J., Troup, E., Burke, B. F., & Ekers, R. D. 1996, *ApJS*, 103, 145

Wright, E. L., et al. 2009, *ApJS*, 180, 283

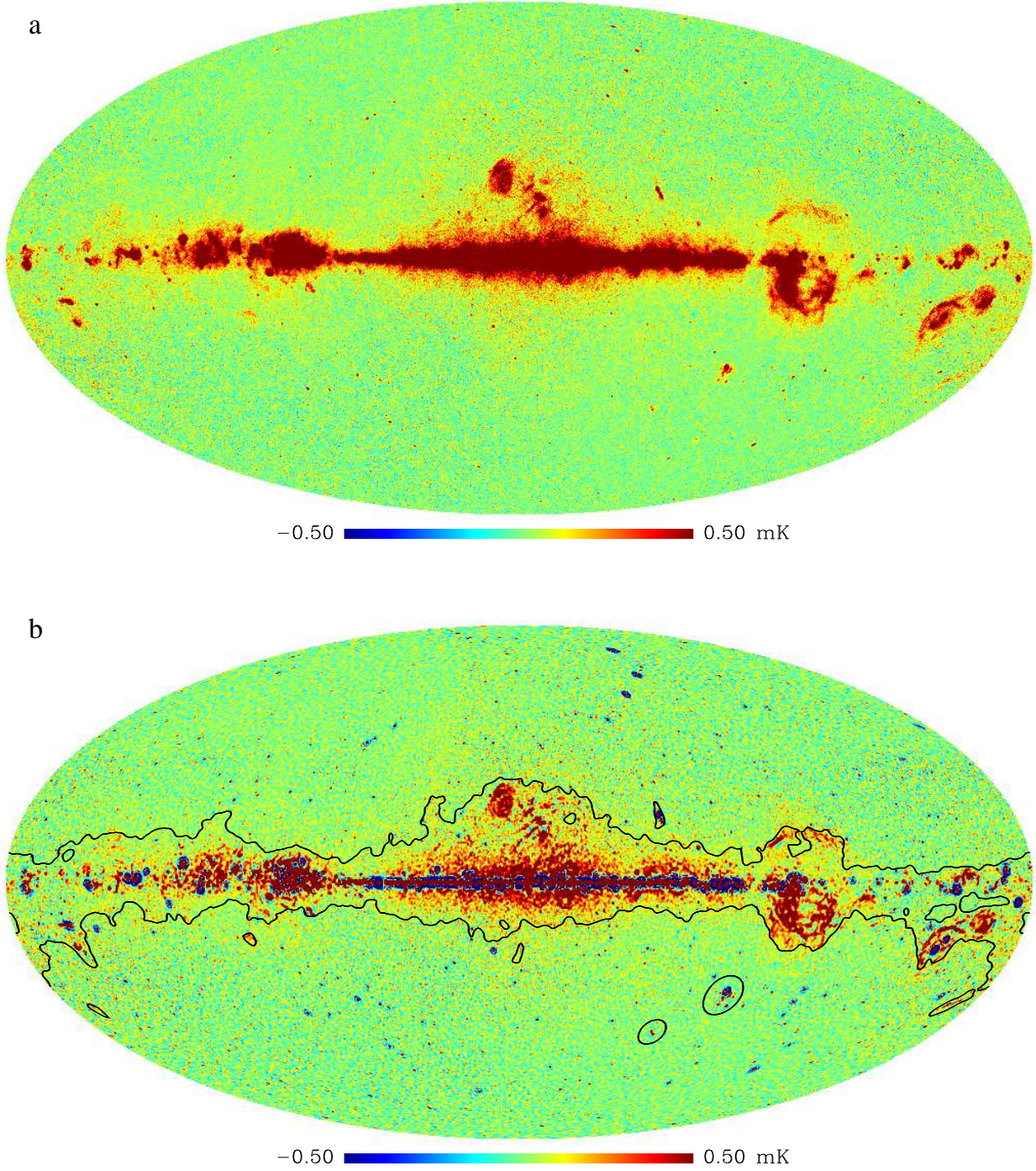


Fig. 1.— (a) The ILC map constructed from the Q-band map, V-band map and W-band map, with the latter two smoothed to Q-band resolution. (b) The filtered ILC map with contours showing the Kp0+LMC+SMC mask used to exclude extended foreground emission.

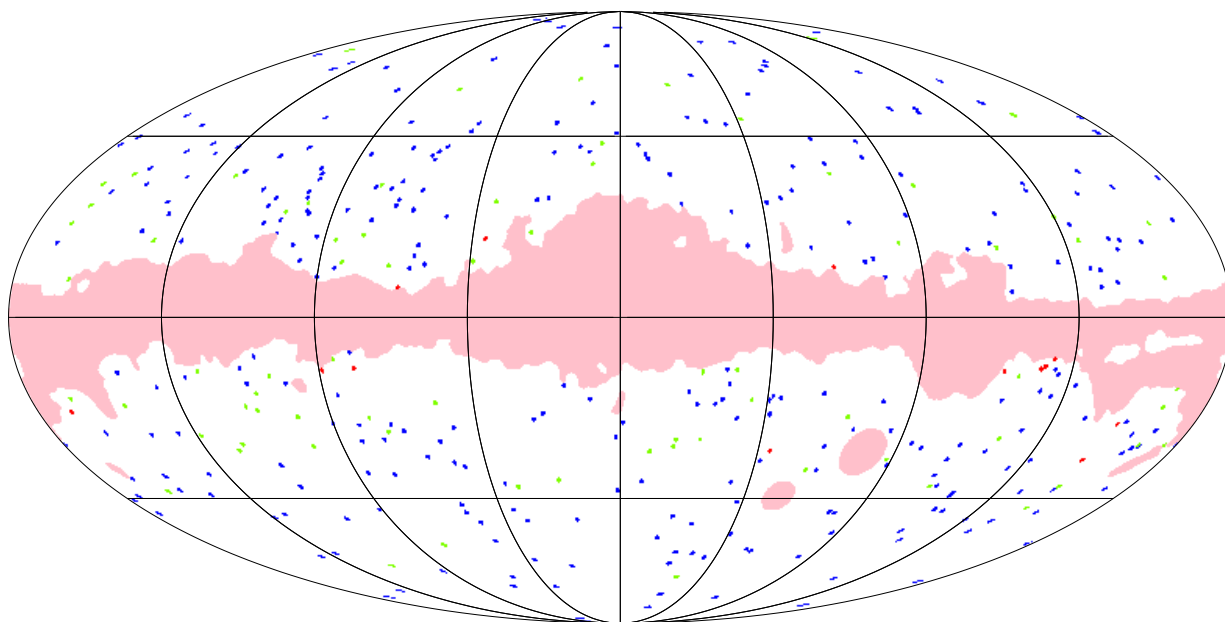


Fig. 2.— Overview map showing the 381 point sources detected in the three-band ILC map. Blue dots represent sources in the WMAP catalogs, green indicates newly detected and identified sources, while red denotes the 14 unidentified sources. The shaded region shows the WMAP point source detection mask.

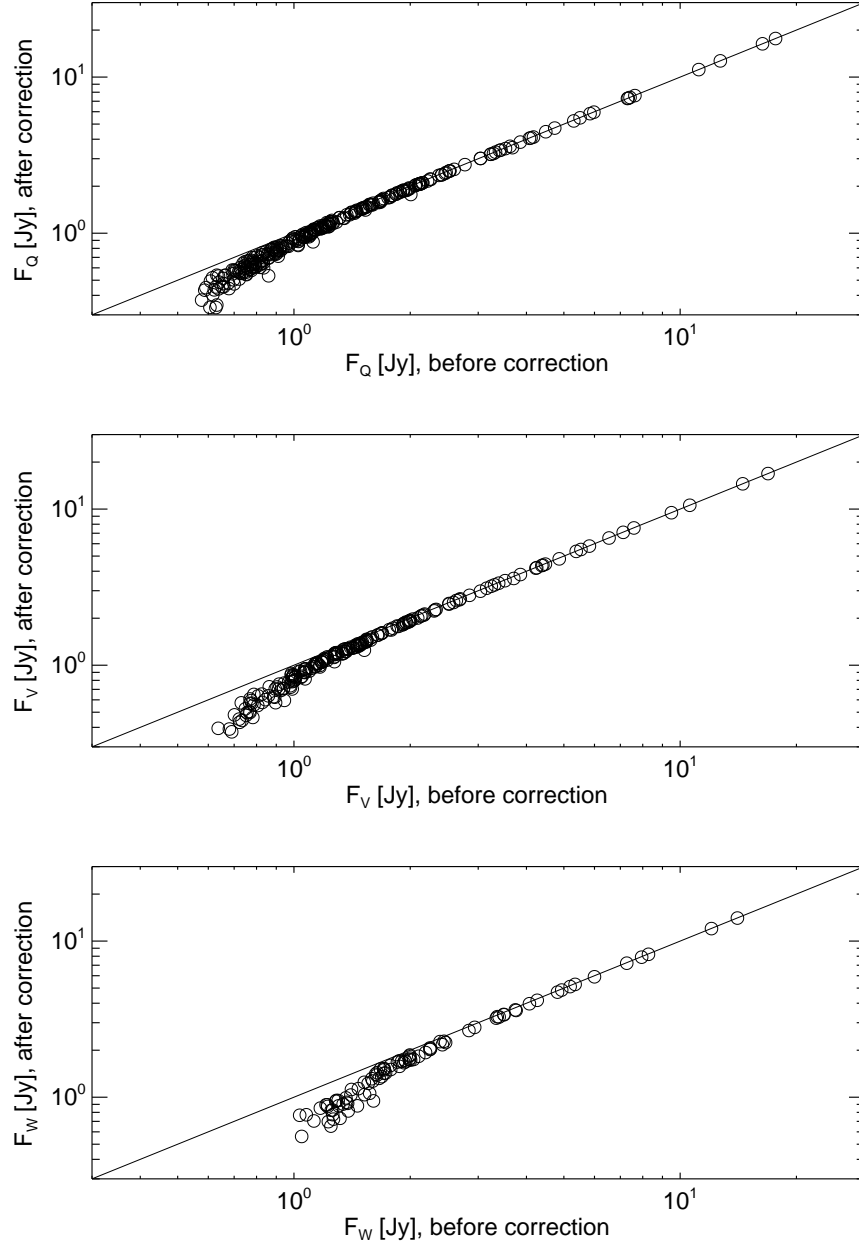


Fig. 3.— Comparison of our flux estimates before and after Bayesian correction.

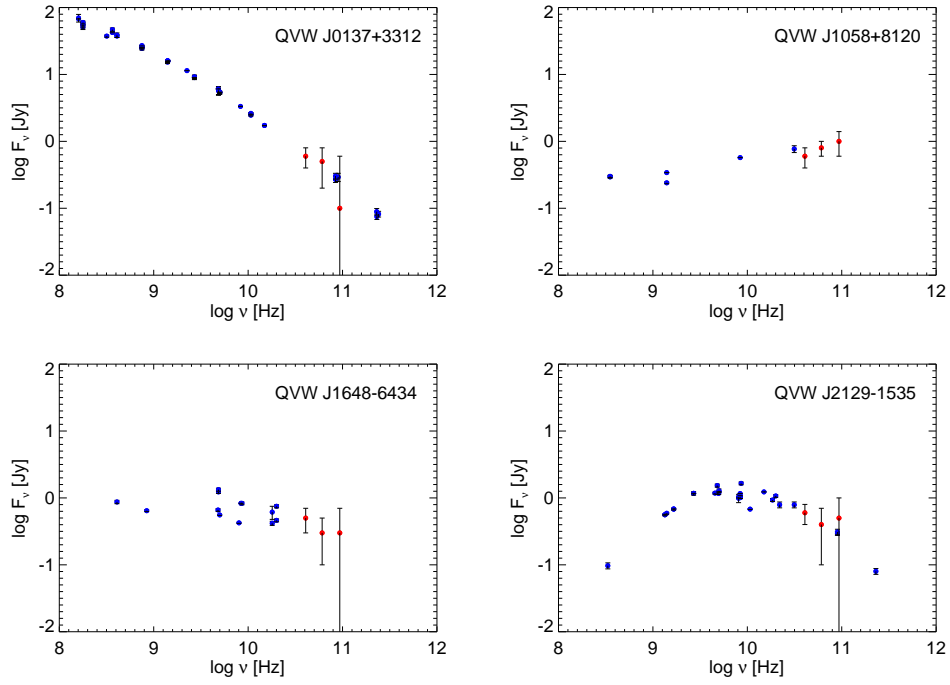


Fig. 4.— Radio spectra examples of our sources. Red and blue dots indicate, respectively, flux estimates obtained in this work and from NED.

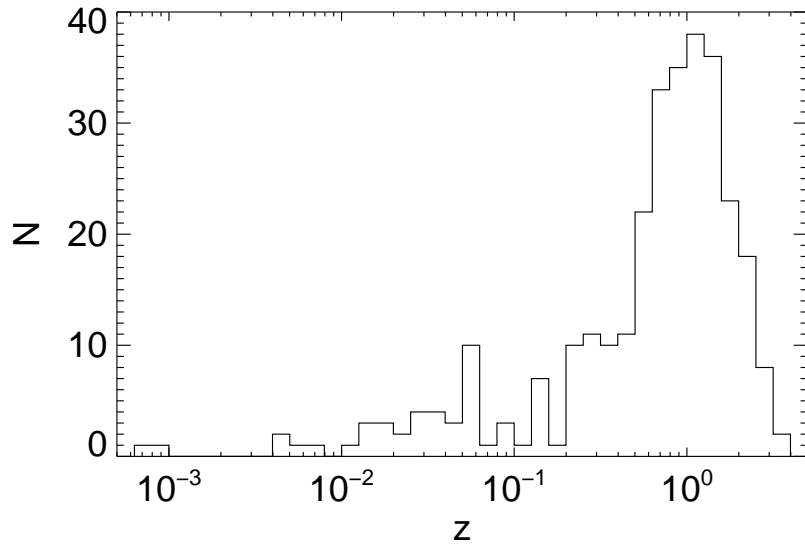


Fig. 5.— Redshift distribution of the 306 sources that have redshift values given in NED. The median of  $z$  is 0.85.



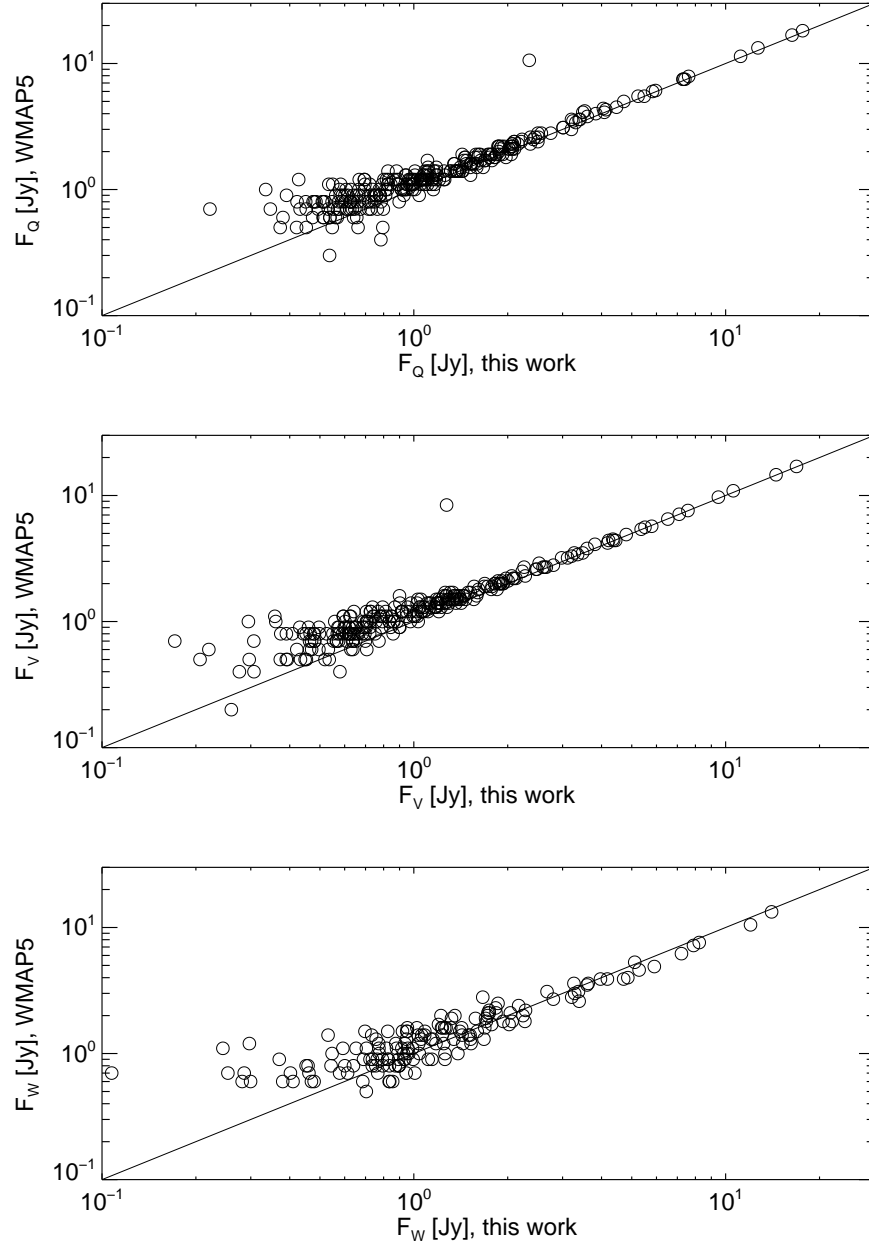


Fig. 6.— Comparison of our flux estimates with WMAP5 flux densities at Q, V and W bands.

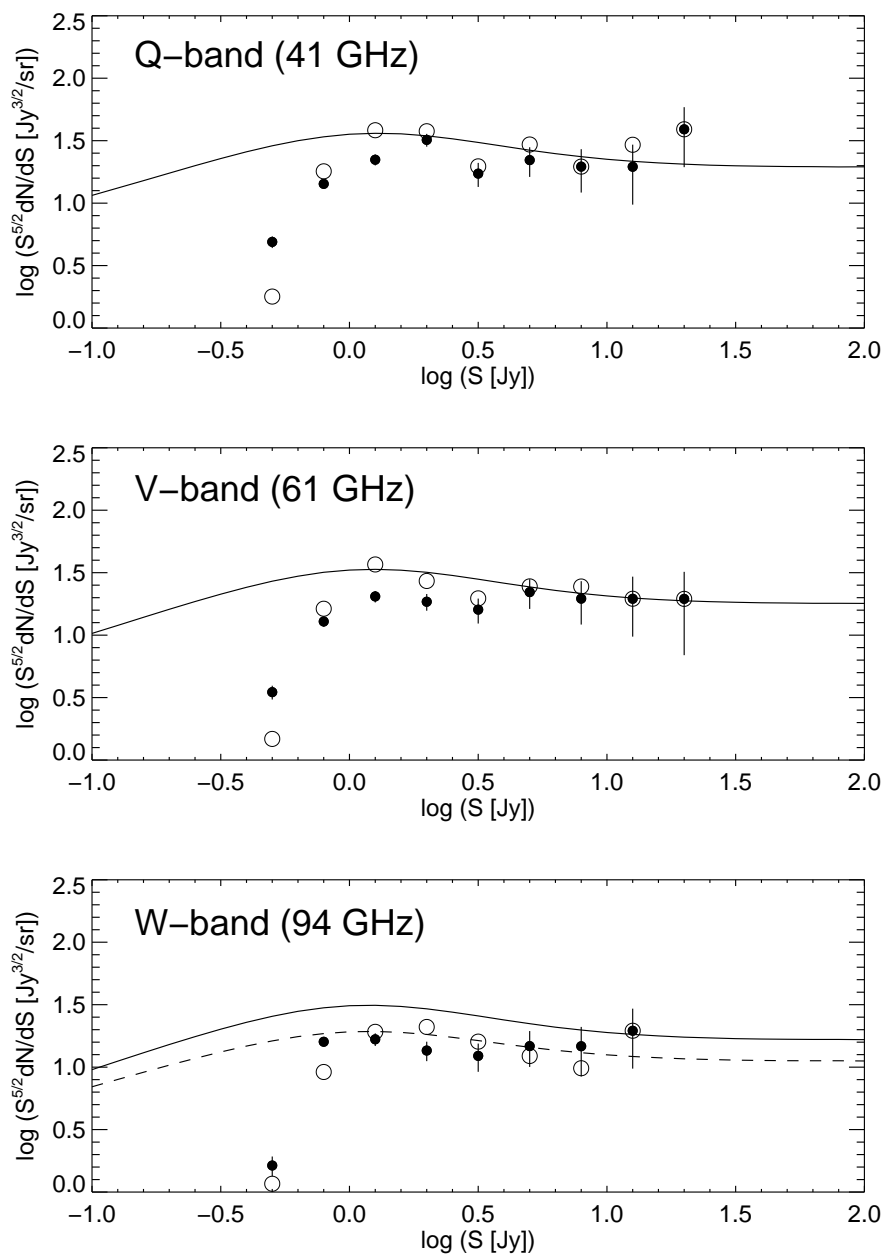


Fig. 7.— Point source counts derived at the Q-, V- and W-band, in bins of  $\Delta \log S = 0.2$ . Sources detected in the ILC map are shown in filled circles with Poisson error bars. Sources in the WMAP5 catalog are shown in big circles for comparison. The curves show the counts predicted by the de Zotti et al. (2005) model. The dashed line in the lowest panel shows the same model scaled by 0.86.

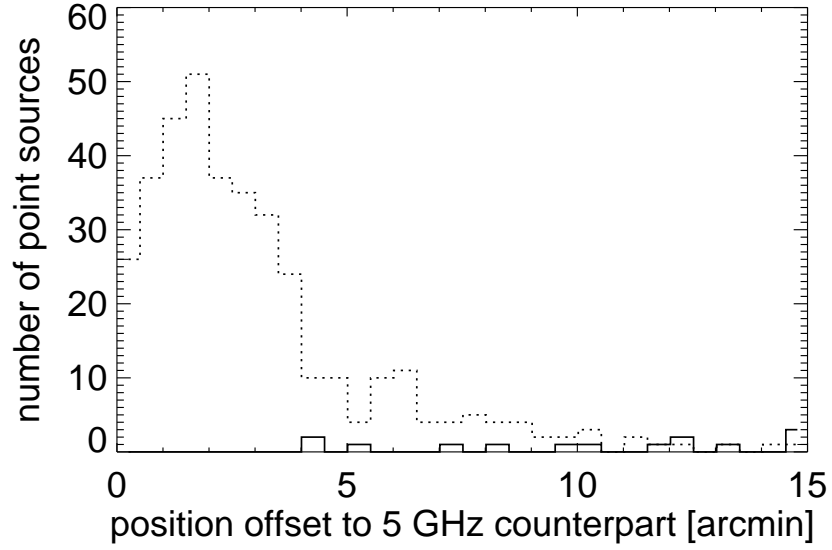


Fig. 8.— Distribution of the deviations from the real detections (dotted line) and false identifications with random positions (solid line) to their 5 GHz counterparts.

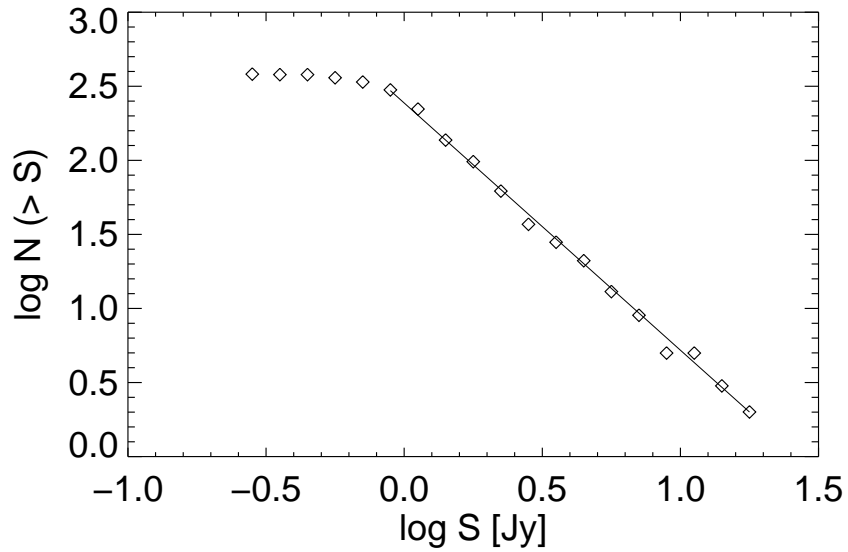


Fig. 9.— Integral counts of extragalactic sources in the WMAP5 Q-band, centered at 40.7 GHz.

Table 1. Point Sources from 5-year Q-, V-, and W-band ILC Map - Identified

RA hms	DEC dm	WMAP ID	Type	Q [Jy]	V [Jy]	W [Jy]	5 GHz ID	Dist. [arcmin]	Note
00 06 13	-06 24	J0006-0623	G	2.4±0.2	1.8±0.3	1.0±0.5	PMN J0006-0623	0.9	b
00 10 34	10 58	J0010+1101	G	1.0±0.2	0.7±0.2	1.3±0.4	GB6 J0010+1058	0.8	b
00 13 05	-39 53	J0012-3952	RadioS	0.7±0.2	1.0±0.2	1.1±0.4	PMN J0013-3954	1.1	b c
00 13 45	40 51	...	G	0.5±0.2	0.6±0.2	0.1±0.4	GB6 J0013+4051	2.6	a b
00 19 40	26 00	J0019+2603	QSO	0.9±0.2	0.4±0.3	0.5±0.4	GB6 J0019+2602	2.1	b
00 19 56	20 20	J0019+2020	RadioS	0.6±0.2	0.8±0.3	-0.4±0.4	GB6 J0019+2021	4.6	b
00 26 04	-35 13	J0026-3510	RadioS	1.4±0.2	1.0±0.2	0.9±0.4	PMN J0026-3512	2.5	b c
00 37 56	-02 07	...	G	0.5±0.2	0.4±0.2	0.9±0.4	PMN J0038-0207	6.1	...
00 38 21	-25 01	J0038-2459	QSO	0.5±0.2	0.8±0.3	0.8±0.4	PMN J0038-2459	3.2	b c
00 47 25	-25 16	J0047-2514	G	1.0±0.2	0.7±0.2	0.7±0.4	PMN J0047-2517	1.9	b
00 48 43	32 00	...	G	0.7±0.2	0.3±0.2	-0.2±0.5	GB6 J0048+3157	3.1	b
00 50 03	-57 36	J0049-5739	QSO	1.1±0.2	1.1±0.2	0.9±0.4	PMN J0050-5738	2.5	b c
00 57 44	30 26	...	G	1.0±0.2	0.6±0.2	0.3±0.4	GB6 J0057+3021	5.7	b
00 59 24	-56 56	J0100-5654	QSO	0.5±0.2	0.4±0.2	0.2±0.4	PMN J0058-5659	5.6	b c
01 06 46	-40 33	J0106-4035	QSO	2.0±0.2	1.9±0.2	1.4±0.4	PMN J0106-4034	1.2	b c
01 08 28	13 21	J0108+1319	GPair	0.6±0.2	0.5±0.3	-0.5±0.4	GB6 J0108+1319	6.3	...
01 08 34	01 36	J0108+0135	QSO	1.7±0.2	1.4±0.3	0.4±0.4	GB6 J0108+0135	1.9	b
01 12 59	49 46	...	QSO	0.4±0.2	0.4±0.2	0.1±0.4	GB6 J0113+4948	4.9	b
01 16 20	-11 36	J0116-1137	QSO	1.0±0.2	1.2±0.3	0.6±0.4	PMN J0116-1136	1.8	b
01 21 51	11 52	J0121+1150	QSO	1.2±0.2	0.5±0.2	0.2±0.4	GB6 J0121+1149	3.5	b
01 25 31	-00 12	J0125-0010	QSO	0.8±0.2	0.6±0.2	0.6±0.4	PMN J0125-0005	6.5	b
01 32 43	-16 57	J0132-1653	QSO	1.5±0.2	1.4±0.2	1.1±0.4	PMN J0132-1654	2.7	b
01 36 56	47 53	J0137+4753	QSO	3.2±0.2	3.1±0.2	2.1±0.4	GB6 J0136+4751	1.8	b
01 37 25	33 12	...	QSO	0.6±0.2	0.5±0.3	0.1±0.5	GB6 J0137+3309	4.2	...
01 37 30	-24 30	J0137-2428	QSO	1.7±0.2	1.4±0.2	1.1±0.4	PMN J0137-2430	1.9	b c
01 52 19	22 06	J0152+2208	QSO	1.1±0.2	1.3±0.2	1.2±0.4	GB6 J0152+2206	0.3	b
02 04 52	15 14	J0204+1513	QSO	1.0±0.2	1.3±0.2	0.3±0.4	GB6 J0204+1514	0.4	b
02 04 56	-17 04	J0205-1704	QSO	0.8±0.2	0.7±0.2	0.3±0.4	PMN J0204-1701	3.2	b c
02 05 14	32 10	J0205+3213	QSO	1.1±0.2	0.8±0.3	-0.1±0.5	GB6 J0205+3212	2.6	b
02 10 45	-51 01	J0210-5100	QSO	2.7±0.2	2.7±0.2	1.8±0.4	PMN J0210-5101	0.5	b c
02 22 55	43 01	J0223+4303	G	1.4±0.2	1.0±0.2	0.9±0.5	GB6 J0223+4259	3.5	b
02 23 11	-34 40	J0222-3440	QSO	0.5±0.2	0.7±0.2	0.1±0.3	PMN J0222-3441	3.2	b c
02 29 39	-78 43	...	QSO	0.6±0.2	0.1±0.2	0.4±0.4	PMN J0229-7847	4.0	b c
02 31 49	13 19	J0231+1320	QSO	0.8±0.2	0.6±0.3	-0.4±0.4	GB6 J0231+1323	3.9	b
02 37 49	28 48	J0237+2848	QSO	3.2±0.2	3.0±0.3	1.7±0.5	GB6 J0237+2848	0.9	b
02 38 37	16 35	J0238+1637	QSO	1.3±0.2	1.4±0.3	1.3±0.5	GB6 J0238+1637	1.4	b
02 41 11	-08 16	J0241-0821	G	0.6±0.2	0.2±0.2	-0.4±0.4	PMN J0241-0815	1.9	b
02 42 34	11 07	...	QSO	0.7±0.2	0.7±0.3	0.6±0.5	GB6 J0242+1101	7.0	b
02 53 21	-54 41	J0253-5442	QSO	2.2±0.2	2.1±0.2	2.3±0.3	PMN J0253-5441	1.2	b c
02 59 33	-00 16	J0259-0015	QSO	0.7±0.2	0.5±0.2	0.4±0.4	PMN J0259-0020	3.4	b
03 03 39	-62 09	J0303-6212	QSO	1.3±0.2	1.2±0.2	1.0±0.4	PMN J0303-6211	2.1	b c
03 04 59	33 50	...	G	0.6±0.2	0.3±0.3	0.0±0.5	GB6 J0304+3348	4.0	b
03 08 20	04 09	J0308+0405	G	1.1±0.2	0.8±0.3	0.4±0.5	GB6 J0308+0406	3.3	...
03 09 14	10 29	J0309+1028	QSO	1.2±0.2	1.3±0.3	0.9±0.5	GB6 J0309+1029	2.6	b
03 10 00	-60 56	J0309-6102	QSO	0.7±0.2	0.7±0.2	0.5±0.4	PMN J0309-6058	2.0	b c

Table 1—Continued

RA hms	DEC dm	WMAP ID	Type	Q [Jy]	V [Jy]	W [Jy]	5 GHz ID	Dist. [arcmin]	Note
03 11 05	-76 55	J0312-7645	QSO	0.7±0.2	0.5±0.2	0.9±0.4	PMN J0311-7651	4.3	b c
03 12 46	01 31	J0312+0131	QSO	0.6±0.2	0.6±0.2	0.3±0.4	GB6 J0312+0132	1.6	b
03 19 49	41 31	J0319+4131	G	7.3±0.2	5.5±0.2	4.0±0.4	GB6 J0319+4130	0.7	b
03 22 16	-37 11	J0322-3711	G	2.3±0.2	1.3±0.2	0.7±0.3	1Jy 0320-37	5.3	...
03 25 28	22 25	J0325+2225	QSO	0.8±0.2	0.4±0.3	0.2±0.5	GB6 J0325+2223	2.3	b
03 29 51	-23 54	J0329-2354	QSO	1.0±0.2	0.9±0.2	0.7±0.4	PMN J0329-2357	2.4	b c
03 34 06	-40 07	J0334-4007	QSO	1.2±0.2	1.0±0.2	0.7±0.4	PMN J0334-4008	2.0	b c
03 36 50	-13 01	J0336-1257	QSO	0.8±0.2	0.5±0.2	0.3±0.4	PMN J0336-1302	3.7	b
03 39 27	-01 47	J0339-0143	QSO	1.9±0.2	1.3±0.3	2.0±0.4	PMN J0339-0146	1.5	b
03 40 19	-21 22	J0340-2119	QSO	0.8±0.2	0.9±0.2	0.3±0.4	PMN J0340-2119	4.6	b c
03 48 40	-16 09	...	QSO	0.6±0.2	0.8±0.3	0.9±0.4	PMN J0348-1610	0.7	b c
03 48 50	-27 51	J0348-2747	QSO	0.6±0.2	1.0±0.2	0.9±0.4	PMN J0348-2749	3.4	b c
03 58 50	10 22	J0358+1029	G	0.7±0.2	0.3±0.3	0.1±0.5	GB6 J0358+1026	3.9	...
04 02 56	26 02	...	QSO	0.5±0.2	0.7±0.2	-0.1±0.5	GB6 J0403+2600	3.6	b
04 03 54	-36 04	J0403-3604	QSO	3.4±0.2	3.4±0.2	3.3±0.3	PMN J0403-3605	0.3	b
04 05 31	-13 07	J0405-1304	QSO	1.5±0.2	1.2±0.3	0.9±0.4	PMN J0405-1308	1.2	b
04 06 55	-38 24	J0407-3825	QSO	0.7±0.3	0.7±0.3	0.6±0.4	PMN J0406-3826	2.6	b c
04 07 31	07 41	...	QSO	0.8±0.2	0.1±0.3	0.4±0.5	GB6 J0407+0742	1.2	b
04 07 44	-12 16	...	QSO	0.6±0.2	0.8±0.3	-0.2±0.4	PMN J0407-1211	5.3	...
04 11 16	76 55	J0411+7654	G	0.6±0.2	0.7±0.2	0.5±0.4	1Jy 0403+76	2.3	...
04 16 26	-20 49	J0416-2051	QSO	0.6±0.2	0.6±0.2	0.7±0.4	PMN J0416-2056	8.3	...
04 22 55	02 12	J0423+0218	QSO	0.2±0.3	0.5±0.3	-0.1±0.5	GB6 J0422+0219	7.3	b e
04 23 16	-01 20	J0423-0120	QSO	7.6±0.3	7.1±0.3	5.9±0.5	PMN J0423-0120	0.4	b
04 24 25	01 58	...	QSO	0.1±0.3	-0.2±0.3	0.3±0.5	GB6 J0424+0204	7.4	b
04 24 44	00 37	J0424+0035	QSO	2.0±0.6	1.3±0.5	1.0±0.6	GB6 J0424+0036	1.1	b
04 24 47	-37 58	J0424-3757	QSO	1.3±0.2	1.3±0.2	0.9±0.3	PMN J0424-3756	2.0	b c
04 28 53	-37 55	J0428-3757	QSO	1.1±0.2	1.2±0.2	1.4±0.4	PMN J0428-3756	2.5	b c
04 33 18	05 23	J0433+0521	G	2.2±0.2	2.2±0.3	2.2±0.5	GB6 J0433+0521	2.9	b
04 38 56	-45 25	...	RadioS	0.6±0.2	0.1±0.3	0.5±0.4	PMN J0439-4522	3.6	b c
04 40 26	-43 32	J0440-4332	QSO	1.9±0.2	1.5±0.2	0.9±0.4	PMN J0440-4332	1.7	b c
04 42 38	-00 12	J0442-0017	QSO	1.1±0.2	0.7±0.2	0.6±0.5	PMN J0442-0017	5.0	b
04 50 26	-81 02	J0449-8100	QSO	1.6±0.2	1.5±0.2	1.5±0.4	PMN J0450-8100	1.4	b c
04 53 09	-28 08	J0453-2806	QSO	1.0±0.2	1.1±0.2	1.0±0.4	PMN J0453-2807	1.7	b c
04 55 52	-46 16	J0455-4617	QSO	3.8±0.2	3.5±0.2	2.8±0.4	PMN J0455-4616	1.0	b c
04 57 05	-23 24	J0456-2322	QSO	2.5±0.2	1.8±0.2	1.7±0.4	PMN J0457-2324	0.7	b c
04 57 32	06 41	...	G	0.6±0.2	0.7±0.2	0.1±0.5	GB6 J0457+0645	6.8	b
05 01 19	-02 01	J0501-0159	QSO	0.9±0.2	0.7±0.2	0.9±0.5	PMN J0501-0159	2.7	b
05 06 44	-61 08	J0506-6108	QSO	1.5±0.2	0.9±0.2	0.9±0.3	PMN J0506-6109	1.2	c
05 09 56	10 19	...	QSO	0.3±0.2	0.0±0.2	0.0±0.4	GB6 J0509+1012	10.2	b
05 16 43	-62 10	...	QSO	0.6±0.2	0.3±0.2	-0.0±0.3	PMN J0516-6207	3.0	b c
05 19 44	-45 47	J0519-4546	G	4.1±0.2	3.2±0.2	2.3±0.4	1Jy 0518-45	1.1	c
05 23 02	-36 28	J0523-3627	G	3.6±0.2	3.3±0.2	3.4±0.4	PMN J0522-3628	1.1	c
05 23 18	70 30	...	QSO	0.4±0.2	0.2±0.2	-0.1±0.4	GB6 J0524+7034	6.1	b
05 27 19	-12 39	J0527-1241	PN	1.4±0.2	1.0±0.2	1.0±0.4	PMN J0527-1241	3.2	...
05 36 21	-33 58	...	G	0.3±0.2	0.6±0.2	-0.3±0.4	PMN J0536-3401	2.8	b c

Table 1—Continued

RA hms	DEC dm	WMAP ID	Type	Q [Jy]	V [Jy]	W [Jy]	5 GHz ID	Dist. [arcmin]	Note
05 38 49	-44 05	J0538-4405	QSO	5.8±0.2	5.4±0.2	5.3±0.4	PMN J0538-4405	0.3	b c
05 39 49	-28 39	J0539-2844	QSO	0.7±0.1	0.5±0.2	0.4±0.4	PMN J0539-2839	1.2	b c
05 40 51	-54 18	J0540-5415	RadioS	1.3±0.2	1.0±0.2	0.7±0.4	PMN J0540-5418	0.9	b c
05 42 27	47 38	...	RadioS	0.4±0.2	0.2±0.3	0.5±0.5	GB6 J0541+4729	11.3	...
05 50 23	-57 35	J0550-5731	QSO	0.8±0.2	0.6±0.2	0.4±0.4	PMN J0550-5732	3.8	b
06 07 16	67 19	J0607+6723	QSO	0.6±0.2	0.6±0.2	0.0±0.4	GB6 J0607+6720	3.9	b
06 08 54	-22 16	J0608-2220	QSO	0.6±0.2	0.5±0.2	0.7±0.4	PMN J0608-2220	3.6	b c
06 09 38	-15 43	J0609-1541	QSO	3.0±0.2	2.1±0.2	1.5±0.4	PMN J0609-1542	1.2	b c
06 20 21	-25 13	J0621-2516	QSO	0.5±0.2	0.3±0.2	0.2±0.3	PMN J0620-2515	2.8	b c
06 22 52	-64 37	J0623-6436	G	0.5±0.1	0.6±0.2	0.9±0.3	PMN J0623-6436	2.1	b c
06 27 19	-35 28	J0626-3523	G	0.4±0.2	-0.2±0.2	-0.1±0.4	PMN J0627-3529	2.6	b c
06 29 34	-20 00	J0629-1958	RadioS	1.2±0.2	0.7±0.2	0.8±0.4	PMN J0629-1959	2.8	b c
06 35 41	-75 15	J0635-7517	QSO	3.4±0.1	2.5±0.2	1.9±0.3	PMN J0635-7516	0.6	b c
06 36 40	-20 42	J0636-2031	Radios	0.6±0.2	0.3±0.2	0.3±0.4	PMN J0636-2041	1.8	...
06 39 28	73 24	J0639+7327	QSO	0.7±0.1	0.6±0.2	1.0±0.3	GB6 J0639+7324	0.5	b
06 46 31	44 49	J0646+4449	QSO	2.1±0.2	1.4±0.3	1.3±0.4	GB6 J0646+4451	1.9	b
06 48 05	-30 42	...	QSO	0.4±0.2	0.5±0.2	-0.0±0.4	PMN J0648-3044	2.9	b c
07 00 00	17 13	...	RadioS	0.7±0.2	0.3±0.2	-0.1±0.5	GB6 J0700+1709	4.6	...
07 10 36	47 31	...	QSO	0.6±0.2	0.8±0.3	-0.8±0.5	GB6 J0710+4732	1.8	b
07 21 14	04 03	J0720+0403	RadioS	0.4±0.2	0.3±0.2	-0.0±0.4	GB6 J0721+0406	4.3	e
07 21 53	71 19	J0721+7122	QSO	1.8±0.2	1.6±0.2	1.6±0.4	GB6 J0721+7120	0.9	b
07 25 50	-00 52	J0725-0050	G	1.0±0.2	0.8±0.2	0.9±0.5	PMN J0725-0054	2.3	...
07 34 18	50 26	J0734+5021	QSO	0.6±0.2	0.8±0.3	0.6±0.5	GB6 J0733+5022	5.6	b d
07 35 32	-77 15	...	QSO	0.4±0.1	0.0±0.2	0.1±0.4	PMN J0734-7711	4.6	b
07 38 36	17 47	J0738+1743	QSO	0.8±0.2	0.7±0.2	0.3±0.5	GB6 0738+1742	8.5	b
07 39 19	01 38	J0739+0136	QSO	2.1±0.2	2.1±0.2	1.7±0.4	GB6 J0739+0136	1.6	b
07 41 38	31 16	J0741+3111	QSO	0.7±0.2	0.4±0.2	0.1±0.5	GB6 J0741+3112	7.1	b
07 42 38	-67 32	J0743-6727	QSO	0.5±0.2	0.2±0.2	-0.1±0.4	PMN J0743-6726	8.1	b c
07 45 27	10 01	J0745+1016	G	0.6±0.2	0.1±0.3	-0.7±0.5	GB6 J0745+1011	9.4	b
07 46 00	-00 42	J0746-0045	QSO	0.6±0.2	0.6±0.2	0.4±0.5	PMN J0745-0044	2.3	b
07 48 52	24 00	...	QSO	0.6±0.2	0.3±0.3	0.6±0.5	GB6 J0748+2400	3.6	b
07 50 49	12 31	J0750+1230	QSO	2.4±0.2	1.9±0.2	1.9±0.5	GB6 J0750+1231	0.8	b
07 53 07	53 45	J0753+5354	QSO	0.7±0.2	0.6±0.2	0.0±0.5	GB6 J0753+5353	7.6	b
07 56 58	09 54	J0757+0957	QSO	1.6±0.2	1.1±0.2	1.4±0.5	GB6 J0757+0956	2.7	b
08 05 38	61 43	J0805+6133	QSO	0.6±0.2	0.6±0.2	0.3±0.4	GB6 J0805+6144	2.5	b e
08 08 08	49 47	...	QSO	0.5±0.2	0.1±0.3	0.0±0.5	GB6 J0808+4950	6.0	b
08 08 23	-07 50	J0808-0750	QSO	1.0±0.2	1.2±0.2	1.1±0.4	PMN J0808-0751	2.0	b
08 11 26	01 45	...	QSO	0.7±0.2	0.6±0.3	0.5±0.5	GB6 J0811+0146	1.5	b
08 16 41	-24 23	J0816-2425	RadioS	0.6±0.2	0.6±0.2	0.5±0.4	PMN J0816-2421	2.8	c
08 25 05	55 46	...	QSO	0.3±0.2	0.5±0.3	0.1±0.5	GB6 J0824+5552	6.4	b
08 25 07	39 10	J0824+3914	QSO	0.9±0.2	0.6±0.3	0.7±0.5	GB6 J0824+3916	6.1	b
08 25 47	03 08	J0825+0311	QSO	1.6±0.2	1.3±0.3	1.2±0.5	GB6 J0825+0309	1.0	b
08 30 53	24 14	J0831+2411	QSO	1.4±0.3	1.1±0.3	0.9±0.5	GB6 J0830+2410	3.3	b
08 36 33	-20 16	J0836-2015	QSO	2.1±0.2	1.8±0.2	0.8±0.4	PMN J0836-2017	1.6	b c
08 37 31	58 25	J0838+5822	QSO	0.4±0.2	0.6±0.2	0.1±0.4	GB6 J0837+5825	1.1	b

Table 1—Continued

RA hms	DEC dm	WMAP ID	Type	Q [Jy]	V [Jy]	W [Jy]	5 GHz ID	Dist. [arcmin]	Note
08 39 28	01 02	...	QSO	0.6±0.2	0.5±0.3	-0.7±0.5	GB6 J0839+0104	5.9	b
08 40 44	13 12	J0840+1312	QSO	1.6±0.2	0.7±0.3	1.0±0.5	GB6 J0840+1312	0.9	...
08 41 23	70 52	J0841+7053	QSO	1.8±0.2	1.4±0.2	0.7±0.4	GB6 J0841+7053	1.4	b
08 54 54	20 06	J0854+2006	QSO	3.5±0.2	4.2±0.3	3.6±0.5	GB6 J0854+2006	1.2	b
08 58 40	-19 44	...	QSO	0.5±0.2	0.1±0.2	-0.6±0.4	PMN J0858-1950	10.1	b c
09 07 11	-20 21	J0907-2020	RadioS	0.6±0.2	0.3±0.2	-0.4±0.4	PMN J0907-2026	11.2	b
09 09 07	01 23	J0909+0119	QSO	1.9±0.2	1.8±0.3	0.9±0.5	GB6 J0909+0121	1.8	b
09 09 28	42 53	J0909+4253	QSO	1.1±0.2	0.9±0.3	0.6±0.5	GB6 J0909+4253	1.1	...
09 14 28	02 45	J0914+0248	G	0.9±0.3	0.6±0.3	1.1±0.5	GB6 J0914+0245	2.6	b
09 18 13	-12 04	J0918-1203	G	1.0±0.2	0.6±0.2	0.3±0.4	PMN J0918-1205	2.4	...
09 20 53	44 42	J0920+4441	QSO	1.4±0.2	1.0±0.2	0.4±0.4	GB6 J0920+4441	1.2	b
09 21 26	-26 21	J0921-2619	QSO	1.1±0.2	0.9±0.2	0.5±0.4	PMN J0921-2618	3.2	b c
09 21 50	62 19	J0921+6215	QSO	0.9±0.2	0.3±0.2	0.4±0.4	GB6 J0921+6215	3.9	b
09 27 04	39 01	J0927+3901	QSO	5.5±0.2	4.4±0.2	3.2±0.4	GB6 J0927+3902	0.7	b
09 49 00	40 39	J0948+4038	QSO	0.9±0.2	0.9±0.2	1.4±0.4	GB6 J0948+4039	0.9	b
09 55 27	69 40	J0955+6935	G	0.7±0.2	0.8±0.2	0.8±0.4	GB6 J0955+6940	2.2	b
09 56 54	25 19	...	QSO	0.4±0.2	0.3±0.2	0.7±0.4	GB6 J0956+2515	3.9	b
09 58 01	55 26	J0957+5527	QSO	0.7±0.2	0.7±0.2	0.6±0.4	GB6 J0957+5522	4.6	b
09 58 33	47 24	J0958+4722	QSO	1.1±0.2	0.7±0.2	0.7±0.4	GB6 J0958+4725	2.3	b
09 58 37	65 30	J0959+6530	QSO	0.5±0.1	0.5±0.2	0.5±0.4	GB6 J0958+6534	4.0	b
10 15 01	22 58	J1014+2306	QSO	0.8±0.2	0.6±0.2	0.2±0.4	GB6 J1014+2301	4.0	b e
10 35 16	-20 16	...	QSO	0.3±0.2	0.3±0.2	-0.2±0.4	PMN J1035-2011	6.0	b c
10 37 18	-29 36	J1037-2934	QSO	1.4±0.2	1.3±0.2	2.0±0.4	PMN J1037-2934	2.6	b c
10 37 33	-37 42	...	QSO	0.5±0.2	-0.2±0.2	0.2±0.4	PMN J1036-3744	8.0	b c
10 38 46	05 13	J1038+0510	RadioS	1.1±0.2	1.0±0.3	0.4±0.4	GB6 J1038+0512	1.0	b
10 41 26	06 11	J1041+0611	QSO	1.2±0.2	0.7±0.3	0.5±0.4	GB6 J1041+0610	2.5	b
10 41 28	-47 42	J1041-4738	RadioS	0.5±0.2	0.1±0.2	-0.0±0.4	PMN J1041-4740	3.3	c
10 43 16	24 07	J1043+2407	QSO	0.7±0.2	0.3±0.2	0.6±0.4	GB6 J1043+2408	1.7	b
10 48 05	-19 07	J1047-1909	QSO	1.1±0.2	0.8±0.2	-0.1±0.4	PMN J1048-1909	1.8	b c
10 48 22	71 44	J1047+7143	QSO	1.2±0.2	0.9±0.2	0.9±0.4	GB6 J1048+7143	1.2	b
10 58 30	01 34	J1058+0134	QSO	4.5±0.2	4.2±0.2	2.7±0.4	PMN J1058+0133	0.6	b
10 58 55	81 20	...	G	0.6±0.2	0.8±0.2	1.0±0.4	S5 1053+81	6.1	b
10 59 02	-80 04	J1059-8003	QSO	1.9±0.2	2.3±0.2	1.0±0.4	PMN J1058-8003	0.8	b c
11 07 13	-44 52	J1107-4446	QSO	0.9±0.2	0.9±0.2	0.8±0.4	PMN J1107-4449	3.4	b c
11 18 31	-46 33	J1118-4633	QSO	0.3±0.2	0.5±0.2	0.3±0.4	PMN J1118-4634	1.3	c
11 18 54	12 33	J1118+1240	QSO	0.8±0.2	0.6±0.2	0.8±0.4	GB6 J1118+1234	1.5	b
11 26 56	-18 55	J1127-1858	QSO	1.1±0.2	0.8±0.2	1.2±0.4	PMN J1127-1857	2.7	b c
11 30 10	-14 48	J1130-1451	QSO	2.1±0.2	1.2±0.2	0.9±0.4	PMN J1130-1449	0.9	b
11 31 00	38 14	J1130+3814	QSO	1.0±0.2	0.5±0.2	0.8±0.4	GB6 J1130+3815	1.5	b
11 47 07	39 59	...	QSO	0.6±0.2	0.3±0.2	0.9±0.4	GB6 J1146+3958	2.1	b
11 47 09	-38 11	J1147-3811	QSO	1.9±0.2	1.6±0.2	0.8±0.4	PMN J1147-3812	1.6	b c
11 50 14	24 17	...	QSO	0.6±0.2	0.6±0.2	0.1±0.4	GB6 J1150+2417	1.2	b
11 53 13	81 00	J1155+8104	QSO	0.8±0.2	0.8±0.3	0.2±0.4	1Jy 1150+81	1.5	b
11 53 24	49 32	J1153+4932	G	1.9±0.2	1.7±0.2	1.5±0.4	GB6 J1153+4931	1.2	...
11 59 39	29 15	J1159+2915	QSO	2.1±0.2	1.9±0.2	1.7±0.4	GB6 J1159+2914	1.7	b

Table 1—Continued

RA hms	DEC dm	WMAP ID	Type	Q [Jy]	V [Jy]	W [Jy]	5 GHz ID	Dist. [arcmin]	Note
12 03 40	48 04	J1203+4808	G	0.6±0.2	0.5±0.2	0.3±0.4	GB6 J1203+4803	1.9	b
12 05 37	-26 33	...	QSO	0.6±0.2	0.4±0.2	1.0±0.5	PMN J1205-2634	0.9	b c
12 09 18	-24 04	J1209-2403	QSO	0.8±0.2	0.3±0.3	0.1±0.4	PMN J1209-2406	3.9	b c
12 15 53	-17 31	J1215-1729	G	0.9±0.2	0.5±0.2	1.0±0.5	PMN J1215-1731	1.6	b c
12 19 28	05 46	J1219+0549	G	1.9±0.2	1.2±0.3	1.2±0.4	1Jy 1216+06	3.2	b
12 22 22	04 13	J1222+0414	QSO	1.0±0.5	0.7±0.3	1.0±0.4	GB6 J1222+0413	0.2	b
12 29 07	02 03	J1229+0203	QSO	16.3±0.2	14.5±0.3	12.0±0.4	PMN J1229+0203	0.1	b
12 30 49	12 23	J1230+1223	G	12.7±0.2	9.5±0.3	7.2±0.4	GB6 J1230+1223	0.2	...
12 47 02	-25 48	J1246-2547	QSO	1.6±0.2	1.4±0.2	1.1±0.4	PMN J1246-2547	3.6	b c
12 48 29	-46 01	J1248-4600	RadioS	0.8±0.2	0.7±0.2	1.2±0.4	PMN J1248-4559	1.2	b c
12 54 42	11 41	J1254+1142	QSO	0.5±0.2	-0.1±0.3	0.2±0.4	GB6 J1254+1141	0.9	b
12 56 12	-05 47	J1256-0547	QSO	17.7±0.2	16.9±0.2	14.0±0.4	PMN J1256-0547	0.2	b
12 57 59	32 27	J1258+3236	RadioS	0.5±0.2	0.4±0.2	-0.1±0.4	GB6 J1257+3229	1.8	b
12 58 01	-31 53	J1258-3158	QSO	1.1±0.2	0.5±0.2	1.2±0.4	PMN J1257-3154	2.2	b c
12 59 50	51 42	J1259+5141	RadioS	0.6±0.2	0.6±0.2	0.5±0.4	GB6 J1259+5141	3.1	b
13 10 33	32 23	J1310+3222	QSO	2.1±0.2	1.6±0.2	0.9±0.4	GB6 J1310+3220	2.6	b
13 16 08	-33 36	J1316-3337	QSO	1.8±0.2	1.7±0.2	1.4±0.4	PMN J1316-3339	2.7	b c
13 19 13	-12 26	...	RadioS	0.4±0.2	0.4±0.2	-0.4±0.4	PMN J1319-1217	9.1	b
13 26 52	22 06	J1327+2213	QSO	0.6±0.2	0.6±0.2	0.6±0.4	GB6 J1327+2210	4.4	b
13 31 12	30 29	J1331+3030	QSO	1.4±0.2	0.9±0.2	0.6±0.4	GB6 J1331+3030	1.5	...
13 32 48	02 00	J1332+0200	G	0.9±0.2	0.8±0.2	1.2±0.4	GB6 J1332+0200	1.3	b
13 36 37	-34 00	J1336-3358	G	0.7±0.2	0.8±0.2	0.7±0.5	PMN J1336-3358	2.9	b
13 37 41	-12 57	J1337-1257	QSO	6.0±0.2	5.8±0.3	4.7±0.5	PMN J1337-1257	0.3	b
13 44 01	66 04	J1344+6601	QSO	0.4±0.2	0.3±0.2	0.8±0.4	GB6 J1344+6606	1.6	b
13 54 52	-10 42	J1354-1041	QSO	1.1±0.2	1.1±0.2	0.6±0.4	PMN J1354-1041	2.1	b
13 57 10	19 19	J1356+1919	QSO	1.3±0.2	1.3±0.2	1.1±0.4	GB6 J1357+1919	1.4	b
13 59 27	01 59	...	QSO	0.5±0.2	0.5±0.2	0.8±0.4	GB6 J1359+0159	0.4	b
13 59 36	76 46	J1355+7647	QSO	0.8±0.2	0.4±0.2	0.2±0.4	S5 1357+76	6.5	...
14 08 57	-07 49	J1408-0749	QSO	0.8±0.2	0.4±0.3	0.9±0.4	1Jy 1406-076	2.5	...
14 15 52	13 14	J1415+1322	QSO	0.5±0.2	0.4±0.2	-0.3±0.4	GB6 J1415+1320	6.1	b
14 19 59	38 24	J1419+3822	QSO	0.7±0.1	1.1±0.2	0.9±0.3	GB6 J1419+3822	3.3	b
14 20 08	54 26	J1419+5425	QSO	0.6±0.2	1.1±0.2	0.9±0.3	GB6 J1419+5423	4.5	b
14 27 32	-33 03	J1427-3302	RadioS	1.6±0.2	1.3±0.2	0.9±0.5	PMN J1427-3306	3.1	b c
14 27 58	-42 04	J1427-4206	QSO	2.6±0.2	2.3±0.2	1.3±0.4	PMN J1427-4206	2.0	b c
14 46 28	17 23	...	QSO	0.5±0.2	0.4±0.2	0.9±0.4	GB6 J1446+1721	3.0	b
14 58 56	71 41	J1458+7140	QSO	0.8±0.2	0.7±0.2	0.8±0.4	GB6 J1459+7140	1.6	...
15 04 33	10 25	J1504+1030	QSO	1.1±0.2	0.6±0.2	1.3±0.4	GB6 J1504+1029	4.3	b
15 07 12	42 41	...	QSO	0.4±0.2	0.4±0.2	0.6±0.4	GB6 J1506+4239	4.2	b
15 07 15	-16 55	J1506-1644	QSO	0.9±0.2	0.4±0.2	0.4±0.4	PMN J1507-1652	3.8	b c
15 10 44	-05 43	J1510-0546	QSO	1.0±0.2	0.6±0.2	0.9±0.4	PMN J1510-0543	2.4	...
15 12 45	-09 05	J1512-0904	QSO	1.9±0.2	1.7±0.3	1.7±0.4	1Jy 1510-08	1.6	...
15 13 43	-10 13	J1514-1013	QSO	0.5±0.3	0.9±0.3	0.9±0.4	PMN J1513-1012	2.0	b d
15 16 40	00 12	J1516+0014	G	1.1±0.2	1.3±0.2	1.0±0.4	GB6 J1516+0015	2.2	b
15 17 43	-24 24	J1517-2421	G	2.1±0.2	1.9±0.2	1.8±0.5	PMN J1517-2422	1.8	b c
15 34 49	01 25	...	QSO	0.6±0.2	0.5±0.2	0.1±0.4	GB6 J1534+0131	5.8	b



Table 1—Continued

RA hms	DEC dm	WMAP ID	Type	Q [Jy]	V [Jy]	W [Jy]	5 GHz ID	Dist. [arcmin]	Note
15 40 56	14 48	J1540+1447	QSO	0.7±0.2	0.6±0.2	0.4±0.4	GB6 J1540+1447	1.7	b
15 49 17	50 35	J1549+5036	QSO	0.9±0.2	0.6±0.2	0.4±0.4	GB6 J1549+5038	2.8	b
15 49 34	02 35	J1549+0236	QSO	2.1±0.2	2.0±0.3	1.7±0.4	GB6 J1549+0237	2.0	b
15 50 35	05 28	J1550+0526	QSO	1.6±0.2	1.9±0.3	1.4±0.4	GB6 J1550+0527	1.0	b
15 53 29	-79 14	J1556-7912	G	0.5±0.2	-0.3±0.2	-0.6±0.4	PMN J1556-7914	9.8	b c d
15 57 53	-00 06	...	QSO	0.5±0.2	0.6±0.3	0.1±0.4	PMN J1557-0001	4.6	b
16 02 07	33 26	J1601+3329	G	0.5±0.2	0.5±0.2	0.6±0.4	GB6 J1602+3326	0.5	b
16 08 41	10 28	J1608+1027	QSO	1.6±0.2	1.4±0.2	1.0±0.4	GB6 J1608+1029	1.4	b
16 13 43	34 12	J1613+3412	QSO	3.3±0.2	2.8±0.2	1.7±0.3	GB6 J1613+3412	0.5	b
16 17 44	-77 17	J1618-7716	QSO	1.7±0.2	1.5±0.2	0.8±0.4	PMN J1617-7717	0.6	b c
16 34 09	82 27	J1633+8226	G	1.2±0.2	0.7±0.2	0.9±0.4	S5 1637+82	5.7	...
16 35 20	38 08	J1635+3807	QSO	3.5±0.4	3.6±0.4	3.4±0.4	GB6 J1635+3808	0.9	b
16 37 43	47 13	J1637+4713	QSO	0.9±0.2	0.7±0.2	0.8±0.4	GB6 J1637+4717	3.7	b
16 38 27	57 19	J1638+5722	QSO	1.4±0.2	1.5±0.2	1.0±0.4	GB6 J1638+5720	1.9	b
16 41 56	68 57	J1642+6854	QSO	1.7±0.2	1.3±0.2	1.0±0.3	GB6 J1642+6856	1.2	b
16 42 59	39 48	J1642+3948	QSO	5.2±0.4	4.8±0.3	4.2±0.4	GB6 J1642+3948	0.4	b
16 44 52	-77 13	J1643-7712	G	0.6±0.2	0.6±0.2	0.8±0.4	PMN J1644-7715	3.4	b d
16 48 21	-64 34	...	RadioS	0.5±0.2	0.3±0.2	0.3±0.4	PMN J1647-6437	6.0	b c
16 48 45	41 09	J1648+4114	QSO	0.4±0.5	0.1±0.4	0.4±0.4	GB6 J1648+4104	6.5	b d
16 51 06	04 57	J1651+0458	G	1.2±0.2	0.5±0.2	0.2±0.4	GB6 J1651+0459	1.7	...
16 53 58	39 47	J1654+3939	G	0.7±0.4	0.5±0.4	0.6±0.4	GB6 J1653+3945	2.3	b
16 58 05	07 38	J1658+0742	QSO	1.1±0.2	0.9±0.2	1.0±0.5	GB6 J1658+0741	2.8	b
16 59 54	68 30	J1659+6827	G	0.5±0.2	0.6±0.2	0.5±0.3	GB6 J1700+6830	1.4	b
17 03 20	-62 13	J1703-6214	RadioS	1.4±0.2	1.2±0.2	1.2±0.4	PMN J1703-6212	2.2	b c
17 15 32	68 40	J1715+6839	QSO	0.5±0.1	0.4±0.2	0.4±0.3	GB6 J1716+6836	5.4	b
17 19 10	17 43	...	QSO	0.4±0.2	0.6±0.2	1.0±0.4	GB6 J1719+1745	1.8	b
17 23 50	-64 57	J1724-6500	G	1.3±0.2	1.0±0.2	1.2±0.4	PMN J1723-6500	2.9	b c
17 26 17	-72 54	...	G	0.4±0.2	0.3±0.2	0.2±0.4	PMN J1726-7259	5.3	b
17 27 28	45 27	J1727+4530	QSO	0.5±0.2	0.7±0.2	0.7±0.4	GB6 J1727+4530	3.2	b
17 28 22	04 29	...	QSO	1.0±0.2	0.9±0.2	0.4±0.4	GB6 J1728+0426	2.5	b
17 34 24	38 56	J1734+3857	QSO	1.1±0.2	1.1±0.2	1.0±0.4	GB6 J1734+3857	1.2	b
17 34 56	-79 36	J1736-7934	QSO	0.8±0.2	0.6±0.2	0.8±0.4	PMN J1733-7935	3.4	b c
17 35 55	50 56	...	G	0.2±0.2	-0.1±0.2	-0.3±0.4	GB6 J1735+5048	7.4	b
17 37 43	-56 35	...	G	0.6±0.2	0.1±0.2	0.3±0.4	PMN J1737-5633	1.6	...
17 40 05	47 39	J1740+4740	QSO	0.8±0.2	0.4±0.2	0.6±0.3	GB6 J1739+4738	2.1	b
17 40 27	52 11	J1740+5212	QSO	1.2±0.2	1.1±0.2	0.7±0.4	GB6 J1740+5211	1.5	b
17 48 50	70 06	J1748+7006	QSO	0.6±0.2	0.9±0.2	0.8±0.3	GB6 J1748+7005	1.5	b
17 53 06	44 07	J1753+4408	QSO	0.6±0.2	0.6±0.2	0.6±0.4	GB6 J1753+4410	3.6	b
17 53 52	28 48	J1753+2848	RadioS	1.9±0.2	2.0±0.2	1.0±0.4	GB6 J1753+2847	2.2	b
17 56 46	15 34	...	RadioS	0.5±0.2	0.2±0.2	0.1±0.4	GB6 J1756+1535	1.7	b
18 00 07	78 28	J1800+7827	QSO	1.5±0.2	1.2±0.2	0.9±0.4	1Jy 1803+78	2.1	b
18 00 13	38 46	J1759+3852	QSO	0.7±0.2	0.2±0.2	0.1±0.4	GB6 J1800+3848	3.0	b
18 01 28	44 04	J1801+4404	QSO	1.5±0.2	1.4±0.2	0.9±0.4	GB6 J1801+4404	0.8	b
18 03 10	-65 08	J1803-6507	RadioS	1.0±0.2	0.8±0.2	1.0±0.4	PMN J1803-6507	1.6	b c
18 06 45	69 48	J1806+6949	G	1.2±0.1	1.2±0.2	0.8±0.3	GB6 J1806+6949	0.8	b

Table 1—Continued

RA hms	DEC dm	WMAP ID	Type	Q [Jy]	V [Jy]	W [Jy]	5 GHz ID	Dist. [arcmin]	Note
18 19 36	-63 47	J1820-6343	G	0.8±0.2	1.1±0.2	0.9±0.4	PMN J1819-6345	1.7	c
18 20 02	-55 19	J1819-5521	QSO	0.6±0.2	0.4±0.2	0.2±0.4	PMN J1819-5521	3.2	c
18 22 40	15 56	...	RadioS	0.4±0.2	0.4±0.2	0.1±0.4	GB6 J1822+1600	8.0	b
18 23 10	68 54	...	RadioS	0.2±0.2	0.2±0.2	-0.0±0.3	GB6 J1823+6857	4.1	b
18 24 03	56 50	J1824+5650	QSO	1.3±0.2	1.1±0.2	0.9±0.4	GB6 J1824+5650	1.0	...
18 29 40	48 44	J1829+4845	QSO	2.5±0.2	1.9±0.2	1.7±0.4	GB6 J1829+4844	1.4	b
18 34 32	-58 55	J1834-5854	QSO	1.0±0.2	0.4±0.2	0.3±0.4	PMN J1834-5856	1.3	b c
18 35 11	32 37	J1835+3245	G	0.7±0.2	0.3±0.2	0.1±0.4	GB6 J1835+3241	4.4	b
18 37 17	-71 06	J1837-7106	QSO	1.1±0.2	0.9±0.2	0.7±0.4	PMN J1837-7108	2.0	b c
18 42 12	79 44	J1840+7946	G	0.7±0.2	0.5±0.2	0.3±0.4	1Jy 1845+79	1.4	b
18 42 31	68 08	J1842+6808	QSO	1.0±0.2	0.8±0.2	0.8±0.3	GB6 J1842+6809	0.9	b
18 48 17	32 17	J1848+3223	QSO	0.8±0.2	0.6±0.2	1.0±0.4	GB6 J1848+3219	2.2	b
18 49 22	67 04	J1849+6705	QSO	1.4±0.2	1.2±0.2	1.5±0.3	GB6 J1849+6705	1.6	b
18 50 24	28 25	J1850+2823	QSO	0.6±0.2	0.5±0.2	0.6±0.4	GB6 J1850+2825	0.8	b
18 52 36	48 47	...	QSO	0.4±0.2	0.2±0.2	-0.1±0.4	GB6 J1852+4855	8.8	b
18 55 45	73 50	...	QSO	0.5±0.2	0.4±0.2	-0.0±0.4	GB6 J1854+7351	3.4	b
19 02 57	31 58	J1902+3153	QSO	0.4±0.2	0.3±0.2	0.2±0.4	GB6 J1902+3159	1.4	b
19 12 33	37 47	...	QSO	0.3±0.2	0.2±0.2	-0.4±0.4	GB6 J1912+3740	6.7	b
19 17 33	55 33	...	RadioS	0.3±0.1	-0.2±0.2	-0.2±0.4	GB6 J1916+5544	12.1	...
19 23 30	-21 04	J1923-2105	QSO	2.4±0.2	2.5±0.2	2.2±0.5	PMN J1923-2104	0.5	b c
19 24 50	-29 14	J1924-2914	QSO	11.2±0.2	10.6±0.2	8.2±0.4	PMN J1924-2914	0.3	b c
19 27 22	61 17	J1927+6119	QSO	0.9±0.1	0.6±0.2	0.5±0.4	GB6 J1927+6117	1.0	b
19 27 59	73 56	J1927+7357	QSO	2.5±0.1	2.6±0.2	1.5±0.4	GB6 J1927+7357	1.6	b
19 37 11	-39 55	J1937-3957	QSO	1.5±0.2	1.2±0.3	0.9±0.5	PMN J1937-3957	2.7	b c
19 41 24	-62 14	...	QSO	0.5±0.2	0.3±0.2	-0.6±0.4	PMN J1941-6211	3.3	b
19 41 55	50 39	...	G	0.5±0.2	0.1±0.2	-0.2±0.4	GB6 J1941+5036	3.8	...
19 46 05	-55 28	...	G	0.3±0.2	-0.1±0.2	-0.8±0.4	PMN J1945-5520	9.7	b c
19 55 56	51 34	J1955+5139	QSO	0.7±0.2	0.4±0.2	0.3±0.4	GB6 J1955+5131	3.5	b
19 58 06	-38 45	J1958-3845	QSO	3.0±0.2	2.6±0.2	1.6±0.5	PMN J1957-3845	1.4	b c
19 58 30	-55 05	...	G	0.4±0.2	0.1±0.2	-0.8±0.5	PMN J1958-5509	4.6	...
20 00 55	-17 48	J2000-1749	QSO	1.5±0.2	1.8±0.2	1.4±0.4	PMN J2000-1748	0.5	b c
20 04 47	77 51	J2005+7755	QSO	0.8±0.2	0.4±0.2	1.1±0.4	1Jy 2007+77	2.7	b
20 07 25	66 07	J2008+6612	QSO	0.4±0.2	0.5±0.2	0.0±0.3	GB6 J2007+6607	0.5	b
20 09 22	-48 46	...	QSO	0.6±0.2	0.7±0.2	0.2±0.4	PMN J2009-4849	3.9	b c
20 09 54	72 31	J2010+7231	QSO	0.9±0.1	0.9±0.2	0.6±0.4	GB6 J2009+7229	1.8	b
20 11 13	-15 43	J2011-1547	QSO	1.5±0.2	1.0±0.3	0.7±0.5	PMN J2011-1546	3.3	b c
20 22 19	61 37	J2022+6136	G	1.1±0.2	0.6±0.2	0.1±0.4	GB6 J2022+6137	1.6	b
20 23 51	54 35	J2023+5426	RadioS	0.5±0.2	0.6±0.2	0.3±0.4	GB6 J2023+5427	8.3	...
20 49 27	10 12	...	RadioS	0.5±0.2	-0.2±0.2	0.6±0.4	GB6 J2049+1003	10.3	b
20 56 12	-47 15	J2056-4716	QSO	2.1±0.2	2.1±0.2	1.8±0.4	PMN J2056-4714	1.0	b c
21 01 34	03 39	J2101+0344	QSO	0.9±0.2	0.7±0.3	0.7±0.5	GB6 J2101+0341	2.6	b
21 06 50	-25 21	...	GTrpl	0.6±0.2	0.5±0.3	-0.1±0.4	PMN J2107-2526	8.9	b
21 09 16	35 33	J2109+3537	G	0.5±0.2	0.4±0.2	0.3±0.3	GB6 J2109+3532	3.2	...
21 09 21	-41 06	J2109-4113	QSO	1.1±0.2	0.6±0.2	0.8±0.4	PMN J2109-4110	4.8	b c
21 23 39	05 34	J2123+0536	QSO	1.8±0.2	1.0±0.2	0.7±0.4	GB6 J2123+0535	1.8	b

Table 1—Continued

RA hms	DEC dm	WMAP ID	Type	Q [Jy]	V [Jy]	W [Jy]	5 GHz ID	Dist. [arcmin]	Note
21 29 10	-15 35	...	QSO	0.6±0.2	0.4±0.3	0.5±0.5	PMN J2129-1538	3.4	b c
21 31 39	-12 08	J2131-1207	QSO	2.2±0.2	1.3±0.2	1.3±0.4	PMN J2131-1207	2.1	b
21 33 30	38 04	...	RadioS	0.2±0.2	0.2±0.2	-0.3±0.4	GB6 J2133+3812	9.0	...
21 34 10	-01 55	J2134-0154	QSO	1.7±0.2	1.4±0.3	1.1±0.4	PMN J2134-0153	1.8	b
21 36 36	00 41	J2136+0041	QSO	3.2±0.2	1.4±0.2	0.7±0.4	GB6 J2136+0041	0.8	b
21 39 09	14 24	J2139+1425	QSO	1.4±0.2	1.0±0.2	0.9±0.4	GB6 J2139+1423	2.2	b
21 43 00	17 45	J2143+1741	QSO	0.3±0.2	0.5±0.2	0.7±0.4	GB6 J2143+1743	8.6	b
21 46 33	-77 59	J2148-7758	QSO	0.9±0.2	0.6±0.2	0.0±0.4	PMN J2146-7755	3.4	b c
21 48 04	06 57	J2148+0657	QSO	7.4±0.2	6.5±0.2	5.1±0.4	GB6 J2148+0657	0.4	b c
21 51 57	-30 28	J2151-3027	QSO	1.3±0.2	1.4±0.2	0.8±0.5	PMN J2151-3028	0.9	b c
21 52 15	17 36	...	QSO	0.6±0.2	0.5±0.2	0.3±0.4	GB6 J2152+1734	2.9	b
21 54 59	23 01	...	RadioS	0.5±0.2	0.1±0.2	-0.2±0.4	GB6 J2155+2250	11.6	b
21 57 02	-69 40	J2157-6942	G	2.4±0.2	1.9±0.2	0.8±0.4	PMN J2157-6941	1.0	c
21 58 12	-15 02	J2158-1501	QSO	1.6±0.2	1.2±0.3	0.9±0.4	PMN J2158-1501	2.2	b c
22 03 16	31 45	J2203+3146	QSO	2.0±0.2	1.6±0.2	1.2±0.4	GB6 J2203+3145	0.4	b
22 03 25	17 26	J2203+1723	QSO	1.5±0.2	1.6±0.2	0.8±0.4	GB6 J2203+1725	0.7	b
22 06 04	-18 36	J2206-1838	QSO	0.7±0.2	0.8±0.2	0.6±0.4	PMN J2206-1835	1.8	b c
22 07 40	-53 43	J2207-5348	QSO	0.6±0.2	0.3±0.2	0.2±0.4	PMN J2207-5346	2.8	b c
22 11 54	23 54	J2211+2352	QSO	0.8±0.2	0.8±0.2	0.7±0.4	GB6 J2212+2355	2.9	b
22 18 59	-03 35	J2218-0335	QSO	1.8±0.4	1.2±0.4	0.8±0.5	PMN J2218-0335	1.8	b
22 25 31	21 17	J2225+2119	QSO	0.6±0.2	0.7±0.2	0.7±0.4	GB6 J2225+2118	1.8	b
22 25 48	-04 57	J2225-0455	QSO	4.1±0.3	3.8±0.3	3.3±0.4	PMN J2225-0457	0.2	b
22 29 37	-08 30	J2229-0833	QSO	2.1±0.2	2.5±0.3	1.7±0.5	PMN J2229-0832	2.9	b
22 32 34	11 42	J2232+1144	QSO	4.1±0.2	4.3±0.2	4.9±0.4	GB6 J2232+1143	1.1	...
22 35 18	-48 35	J2235-4834	QSO	2.0±0.2	1.9±0.2	1.3±0.4	PMN J2235-4835	0.8	b c
22 36 18	28 31	J2236+2824	QSO	0.9±0.2	0.6±0.2	0.2±0.4	GB6 J2236+2828	3.1	b
22 39 28	-57 00	J2239-5701	RadioS	0.5±0.2	0.7±0.2	0.9±0.3	PMN J2239-5701	2.2	b c
22 46 24	-12 08	J2246-1208	QSO	1.8±0.2	0.9±0.2	0.7±0.4	PMN J2246-1206	2.2	b
22 53 59	16 08	J2254+1608	QSO	7.3±0.2	7.6±0.2	7.9±0.5	GB6 J2253+1608	0.4	b
22 55 35	42 04	J2255+4201	QSO	0.5±0.2	0.2±0.2	-0.3±0.4	GB6 J2255+4202	1.4	b
22 56 44	-20 13	J2256-2014	QSO	0.6±0.2	0.2±0.3	0.3±0.4	PMN J2256-2011	2.3	b c
22 58 07	-27 58	J2258-2757	QSO	4.7±0.2	4.4±0.2	3.6±0.4	PMN J2258-2758	0.3	b c
23 03 45	-68 03	J2302-6808	QSO	0.7±0.2	0.2±0.2	-0.2±0.4	PMN J2303-6807	3.9	b c
23 11 08	34 24	...	QSO	0.4±0.2	0.5±0.2	0.3±0.4	GB6 J2311+3425	0.6	b
23 12 46	45 33	...	QSO	0.3±0.2	-0.2±0.2	-0.9±0.4	GB6 J2311+4543	14.5	b
23 15 49	-50 15	J2315-5018	RadioS	0.7±0.2	0.6±0.2	0.4±0.4	PMN J2315-5018	3.1	b c
23 21 59	51 04	J2322+5105	QSO	0.5±0.1	0.4±0.2	0.4±0.4	GB6 J2322+5057	7.8	...
23 22 09	27 26	...	QSO	0.5±0.2	0.4±0.2	0.3±0.4	GB6 J2322+2732	6.4	b
23 23 41	-03 19	...	QSO	0.7±0.2	0.7±0.3	-0.1±0.4	PMN J2323-0317	3.0	b
23 27 41	09 36	J2327+0937	QSO	1.1±0.2	0.7±0.3	0.8±0.4	GB6 J2327+0940	3.7	b
23 29 24	-47 28	J2329-4733	QSO	1.0±0.2	0.5±0.2	1.1±0.4	PMN J2329-4730	2.1	b c
23 31 48	-16 00	J2331-1558	QSO	0.6±0.2	0.8±0.2	0.8±0.4	PMN J2331-1556	4.1	b c
23 33 35	-23 40	J2333-2340	G	0.6±0.2	0.7±0.2	0.3±0.4	PMN J2333-2343	5.6	b c
23 35 51	-52 42	J2335-5243	QSO	0.4±0.2	0.2±0.2	0.0±0.3	PMN J2336-5236	7.0	b c
23 48 03	-16 30	J2348-1630	QSO	1.7±0.2	1.3±0.3	1.3±0.4	PMN J2348-1631	0.3	b c

Table 1—Continued

RA hms	DEC dm	WMAP ID	Type	Q [Jy]	V [Jy]	W [Jy]	5 GHz ID	Dist. [arcmin]	Note
23 48 06	42 59	...	QSO	0.4±0.2	-0.2±0.2	-0.2±0.4	GB6 J2347+4310	13.5	...
23 54 14	45 54	J2354+4550	QSO	1.0±0.2	0.8±0.2	1.3±0.4	GB6 J2354+4553	2.2	b
23 55 30	49 35	J2356+4953	G	0.0±0.2	0.1±0.2	0.2±0.4	GB6 J2355+4950	14.9	a b
23 57 49	-45 56	...	RadioS	0.3±0.2	0.1±0.2	0.4±0.4	PMN J2358-4555	2.9	b c
23 57 55	-53 08	J2357-5314	QSO	1.2±0.1	0.6±0.2	0.8±0.3	PMN J2357-5311	3.2	b c
23 59 08	-60 56	J2358-6050	G	1.0±0.2	0.6±0.2	0.0±0.4	PMN J2358-6054	1.3	c
23 59 26	39 16	...	QSO	0.6±0.2	0.3±0.2	0.1±0.4	GB6 J2358+3922	7.9	b

<sup>a</sup>The source position is fitted to the local maximum of a  $5 \times 5$  pixel grid as there are two bright pixels within the Q-band beam, both of which are the brightest in their  $3 \times 3$  pixel neighborhood.

<sup>b</sup>Indicates this source is included in the CRATES catalog.

<sup>c</sup>Indicates this source is included in the AT20G BSS catalog.

<sup>d</sup>Indicates the source is in the three-year WMAP point source catalog, but not in the five-year catalog.

<sup>e</sup>The source has a different 5 GHz ID than noted in the WMAP five-year point source catalog.

Table 2. Point Sources from 5-year Q-, V-, and W-band ILC Map - Unidentified

RA hms	DEC dm	Q [Jy]	V [Jy]	W [Jy]	Possible Radio Companion <sup>a</sup>	Dist. [arcmin]	$f_\nu$ <sup>b</sup> [Jy]	Note
03 58 37	22 36	0.4±0.2	0.4±0.3	0.9±0.5	GB6 J0358+2236	0.4	0.074	...
04 34 54	-10 05	0.3±0.2	-0.2±0.2	-0.6±0.4	PMN J0434-1007	4.2	0.121	c
05 03 45	-04 10	0.1±0.2	-0.2±0.3	0.4±0.5	NVSS 050342-041420	3.5	0.079	d
06 43 44	-24 11	-0.0±0.2	-0.1±0.2	0.2±0.4	NVSS J064353-240440	7.4	0.018	...
06 44 28	-23 09	0.2±0.2	0.2±0.2	0.5±0.4	PMN J0644-2322	13.7	0.043	...
06 44 47	-24 34	0.1±0.2	-0.2±0.2	0.2±0.3	NVSS J064419-243804	7.2	0.004	...
06 44 49	-23 31	-0.1±0.2	-0.2±0.2	-0.2±0.4	PMN J0644-2322	8.9	0.043	d
06 47 20	-20 26	0.5±0.2	-0.1±0.2	-0.2±0.4	NVSS J064748-201517	13.1	0.020	...
07 02 06	-34 19	-0.0±0.2	-0.4±0.2	-0.1±0.4	NVSS J070203-341829	1.1	0.019	d
12 10 25	-50 18	0.2±0.2	0.2±0.2	0.1±0.4	SUMSS J120954-501213	8.3	0.012	...
19 28 17	32 31	0.2±0.2	0.2±0.2	0.0±0.4	GB6 J1927+3236	8.5	0.025	...
21 20 46	32 28	0.3±0.2	0.2±0.2	-0.1±0.4	NVSS J212057+322258	5.7	0.010	...
21 29 38	-81 06	0.3±0.2	-0.2±0.2	-0.5±0.4	PMN J2130-8103	4.2	0.088	...
21 56 38	38 27	0.4±0.2	-0.1±0.2	-0.2±0.4	GB6 J2156+3823	6.7	0.027	...

<sup>a</sup>The 5 GHz radio source within 15 arcmin of our source position is given. When a 5 GHz ID is not available, the closest source from NVSS and SUMSS survey is given.

<sup>b</sup>The corresponding flux density of the possible radio companion at 4.85 GHz for PMN and GB6 sources, 1.4 GHz for NVSS sources and 0.843 GHz for SUMSS sources.

<sup>c</sup>This source is in the CRATES catalog, with an 8.4 GHz flux measured at 0.074 Jy.

<sup>d</sup>There are two pixels within one Q-band beam, both of which are the brightest in their  $3 \times 3$  pixel neighborhood. The location showing here is fitted to the local maximum of a  $5 \times 5$  pixel neighborhood including both bright sources.